CHALMERS
UNIVERSITY OF TECHNOLOGY

UNIVERSITY OF GOTHENBURG

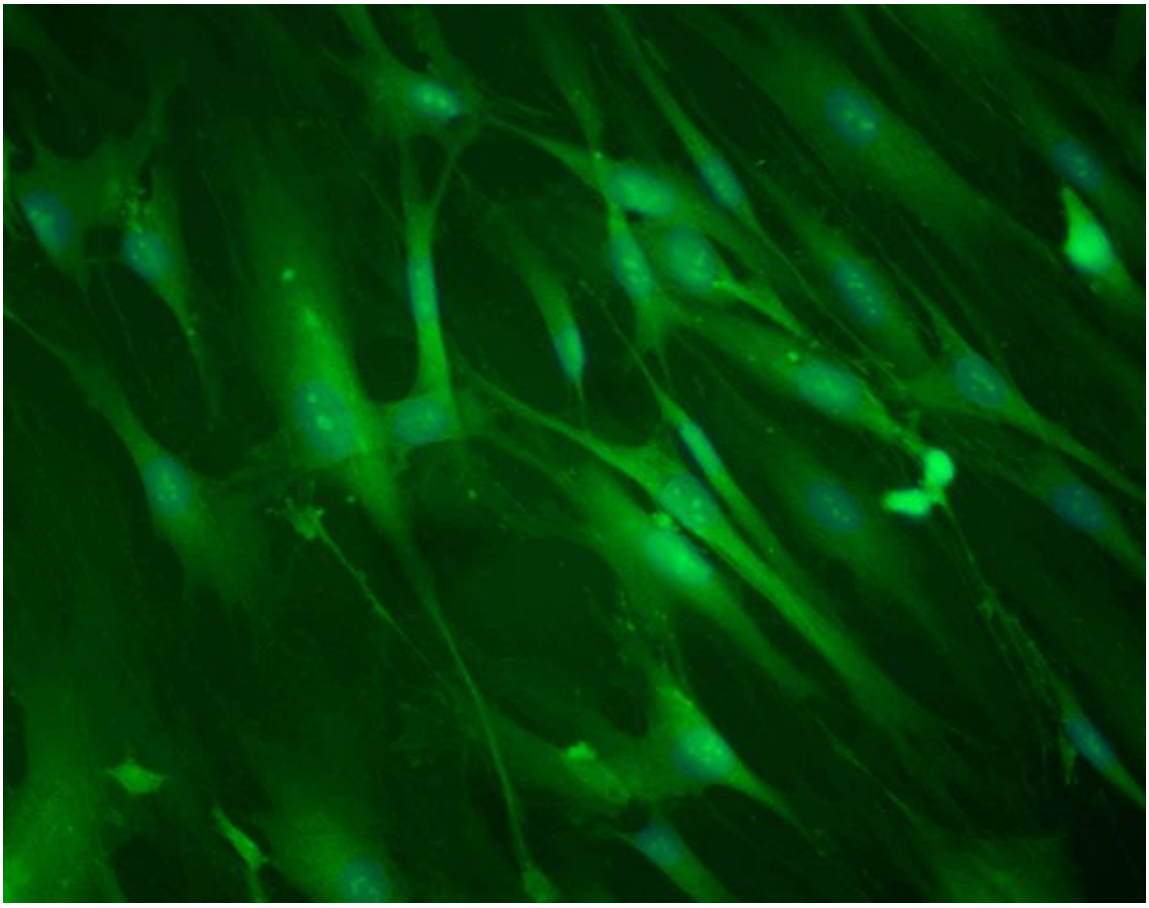

In Vitro Cellular Response to Chemically Modified Titanium Surfaces for Soft Tissue Contact

Master thesis in Material Chemistry and Nanotechnology

ANNA STENBERG

Department of Chemistry and Molecular Biology
UNIVERSITY OF GOTHENBURG
CHALMERS UNIVERSITY OF TECHNOLOGY
DENTSPLY IMPLANTS
Gothenburg, Sweden 2015

DENTSPLY IMPLANTS

Abstract

A dental abutment is the main part of a dental implant pillar with soft tissue contact. It is believed that the composition of the peri-implant mucosa, as well as the soft tissue contact is affected by the abutment surface characteristics. The peri-implant mucosa is mainly made up of connective tissue and epithelium. The production of connective tissue is important during the healing process of a dental implant treatment, and is made of fibroblasts and extracellular matrix.

In this study human gingival fibroblasts (HGF-1) as well as 3T3 mouse fibroblasts were used to evaluate the *in vitro* cellular response to titanium surfaces (Ti), titanium nitride surfaces (TiN) and chemically modified titanium nitride surfaces (TiN_1 and TiN_2). In total four surface groups were evaluated. Ti-sample discs (Ø=6,25 mm) were used for surface characterization using Scanning Electron Microscopy (SEM), contact angle analysis and 2 D stylus profilometry. The *in vitro* cellular response was evaluated in terms of morphology, initial cell adhesion, growth and cell migration using SEM and fluorescence microscopy.

Results showed that the chemical modifications of the titanium surfaces altered the surface characteristics in terms of wettability and morphology. TiN_1-samples showed a higher surface roughness compared to the other samples. The *in vitro* study showed that no difference in the initial adhesion or in the morphology could be observed when comparing the different groups. However, differences between groups were seen when evaluating cell growth and migration. Cell growth was similar for all groups except for TiN_2-samples which did not support cell growth. Cell migration appeared faster for both cell types on TiN-samples as compared to Ti-samples. Migration studies could not be performed on chemically modified titanium nitride samples (TiN_1 and TiN_2), possibly due to poor cell adhesion. The different cell responses obtained for the different groups cannot be related to a single surface modification as the groups showed different surface characteristics in terms of surface roughness, wettability and chemical composition.

Table of contents

1. Introduction

Reasons for patients to need a bone anchored dental implant are usually due to loss of teeth, either as a consequence of disease, or due to a trauma. Today the use of bone anchored dental implants is very common (1). The most common solution before bone anchored dental implants was dentures (2). Dentures are still used today, however, dentures are non-permanent structures and sometimes these structures struggles with issues of fit, comfort or stability (2). On the other hand a bone anchored implant is for permanent use and facilitates a more normal dental function. The use of bone anchored implants has significantly improved the quality of life for patients all over the world (3).

The starting point for bone anchored implants was the discovery of osseointegration. It all started when Per-Ingvar Brånemark in 1950s surgically inserted a titanium screw as a fixture for a dental implant (3). Upon healing he found that a force was required to remove the screw from the bone; the screw had osseointegrated. Osseointegration is the result of bone tissue adhering to the surface of the titanium and permanently incorporating the screw into the bone (3). Upon healing an abutment and crown can be mounted onto the screw completing the implant pillar, see Figure 1.

Figure 1.A three piece bone anchored dental implant. The left hand side of the image shows the three separate structures, the screw, the abutment and the crown. The right hand side of the image illustrated an implant in place. The different structures are in contact with different types of tissues.

Even though osseointegration was a major breakthrough for bone anchored dental implants, in itself, osseointegration is not enough for a successful clinical outcome. Teeth are the only body part which pierces the epithelium (4). By doing so the tooth creates a transmucosal connection between the bone and the oral cavity. Teeth naturally have a barrier sealing off the internal of the body from the external environment in the oral cavity (5). This barrier is established by fibers extending perpendicularly from the root cementum through the periodontal ligament to the underlying bone, see Figure 2 (5). A dental implant on the other hand is inserted straight into the alveolar bone and lacks both root cementum and periodontal ligament, see Figure 2. The absence of these structures causes the tissue surrounding the implant to be different than the tissue surrounding a tooth. For clarifications purposes the term gingiva is only used for tissue surrounding a natural tooth, whereas the tissue surrounding an implant is referred to as peri-implant mucosa.

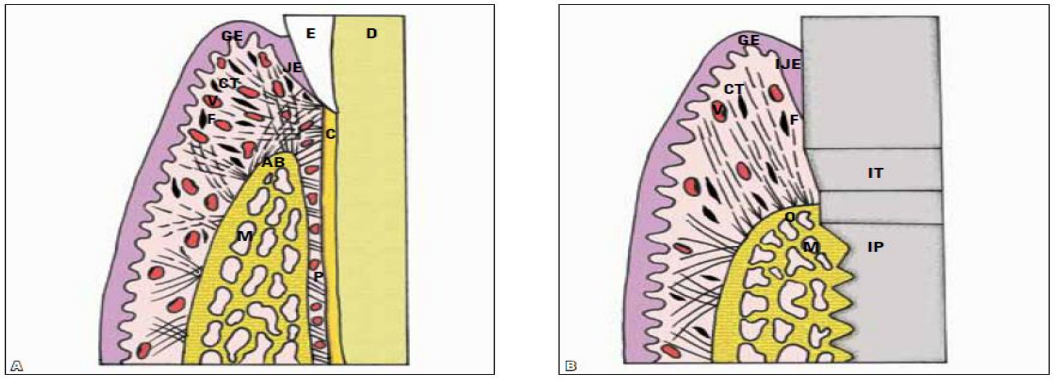

Figure 2. Figure 2A shows the gingival tissue surrounding a natural tooth. The perpendicular fibers extending from the cementum encapsulating the root into the bone tissue provides a seal towards migrating bacteria. Figure 2B shows the peri-implant mucosa surrounding an implant. The horizontal fibers seen in the gingival tissue is missing from the peri-implant structure and thus weakening the barrier towards migrating bactera.

The perpendicular fibers establishing the barrier for teeth cannot be seen in peri-implant mucosa as these structures are destroyed during the surgical procedure, see Figure 2. Instead these fibers run vertically along the side of the abutment, causing the barrier between the body and oral cavity to weaken (5). This makes peri-implant mucosa more susceptible for migrating bacteria from the oral cavity, and consequently also more susceptible for infections (6).

For a successful clinical outcome of a dental implant treatment the establishment of a barrier protecting the bone tissue surrounding the implant from migrating bacteria is essential (7). Poor soft tissue contact does not necessarily result in loss of the implant. However, poor soft tissue contact can result in withdrawal of the peri-implant mucosa leaving part of the abutment exposed in the oral cavity (4). This withdrawal of tissue surrounding the abutment is called apical migration and is usually followed by some extent of bone resorption (5). An exposed abutment results in metal showing through the peri-implant mucosa and causing an esthetic disadvantage for patients (8). Attempts to minimize the effect of apical migration have been to improve the soft tissue contact by modifying the surface characteristics of the abutments, (4) and by changing the color of the abutments and making the abutments less visible through the peri-implant mucosa (8).

Responsible for the soft tissue contact are primarily two different cell types, epithelial cells and fibroblasts. These cell types, in combination with connective tissue, mainly make up the peri-implant mucosa (4). Fibroblasts being more prone to migration, are believed to be responsible for the initial cell adhesion upon insertion of an implant (9). The fibroblasts attach to the implant surface and start to produce proteins which are capable of supporting growth of epithelial cells (10).

Bacteria are plentiful in the oral cavity and these also adhere to an implant structure. Once bacteria adheres to a surface a biofilm is quickly formed, which can be described as a community of bacteria. Once a biofilm is formed it is very hard to remove it and antibiotics may be needed to get rid of the bacteria (11). If a biofilm is formed the implant becomes infected, this can sometimes be treated with antibiotics but in worst case an infection will lead to loss of the implant (12). To avoid formation of biofilms and bacterial adhesion, it is important to ensure that fibroblasts can adhere first and thus protect the implant surface from a bacterial infection (9).

An optimized dental abutment surface needs to balance between protecting surfaces from bacterial adhesion and providing a surface with fibroblasts and epithelial cell adhesion (6). Aiming to reduce bacterial adhesion to the implant, antibacterial surfaces have been researched for dental abutments (12). These surfaces aim to prevent bacterial adhesion, and thereby minimize the need for using

antibiotics. Antibacterial surfaces should target only bacterial cells without affecting the adhesion or proliferation of fibroblasts and epithelial cells.

In published research mainly two approaches to develop antibacterial surfaces have been evaluated (13). The first is a release based mode of action towards bacterial presence in the peri-implant tissue, and involves incorporation of toxins, or antibacterial agents into the implant surface. Once the implant is in place within the body, this toxin is then released into the surrounding environment harming bacteria. To avoid any negative effect on human cells, the concentration of the toxin or antibacterial agent is kept at a concentration lower than what is harmful for human cells. The second approach is a non-adhesive or contact based mode of action, and is thus a surface without the release of toxins or antibacterial agents. These surfaces can either kill bacteria upon contact or prevent bacterial adhesion and thereby reduce the number if bacteria present on the implant surface. An example of such a surface is titanium nitride, TiN, which has shown to have antibacterial properties without the release of toxins or antibacterial agents. TiN surfaces have been found to affect the bacterial adhesion properties negatively without affecting the adhesion properties of fibroblasts or epithelial cells (12).

In this study four different abutments materials will be evaluated in terms of soft tissue contact. The first surface is a pure titanium oxide surface, TiO_2, the second a titanium disc with a TiN coating. These two surfaces serves as reference when evaluating the soft tissue contact. The third and fourth surface are titanium discs with a TiN coating which has been chemically modified.

1.1. Aim

The aim of this study was to evaluate the *in vitro* cellular response to modified titanium surfaces. Four different surface groups were included:

Ti: an uncoated titanium surface used as a control
TiN: a titanium nitride surface, coated with physical vapor deposition, PVD
TiN_1*:a chemically modified TiN-surface[1]
TiN_2: a chemically modified TiN-surface[2]

*This group was included during the course of the study

[1] The exact composition of TiN_1 is only known to Dentsply Implants
[2] The exact composition of TiN_2 is only known to Dentsply Implants

Specific aims to evaluate:

- How do the surface coatings affect the surface properties of the material? Specifically in terms of wettability and surface structure.
- How do the surface coatings affect the cellular response of human gingival fibroblasts, HGF-1 cells and mouse 3T3 cells *in vitro*? Specifically in terms of proliferation, adhesion and migration of the fibroblasts?

1.2. Limitations

- Only surface characteristics of the materials were considered, no mechanical testing was performed.
- The cellular response was evaluated *in vitro* mainly using human gingival fibroblasts.
- The *in vitro* study was performed on experimental samples (flat titanium coins, d = 6, 25 mm) and not on abutments.

2. Literature Study

Implants aimed for use in the human body, usually take inspiration from the natural feature in the body. It aims to be structurally and functionally similar to the structure it is supposed to replace. Keeping this in mind, the understanding of the structural and functional features of the original structure is critical for attempting to design a replacing implant.

2.1. The anatomy of a tooth

Dental implants aim to replace the structure of a tooth. As mentioned previously, the tooth is the only part of the body which pierces the epithelium and creates a sealed transmucosal connection between the internal environment of the body and the external oral cavity (5). A tooth can structurally and functionally be divided into three different sections: the root, the neck and the crown, see Figure 3. Depending on the location in the oral cavity the root anchors the tooth to the upper or lower jawbone. It also encloses the root canals, which enables nerves and blood vessels to reach the pulp cavity.

The neck is in direct contact with the surrounding gingiva, and is responsible for maintaining the transmucosal barrier discussed in the introduction, see Figure 2. The top part of the tooth is the crown. This is normally the only visible part of a tooth and it is encapsulated by enamel, the hardest substance found in the body (14). The enamel covers an underlying layer of dentin, a calcium rich connective tissue substance. The dentin provides the tooth with its shape and rigidity. The pulp cavity is located inside the crown and has a high density of blood vessels and nerves, which extend canals throughout the tooth which supports the cells in the structure (14).

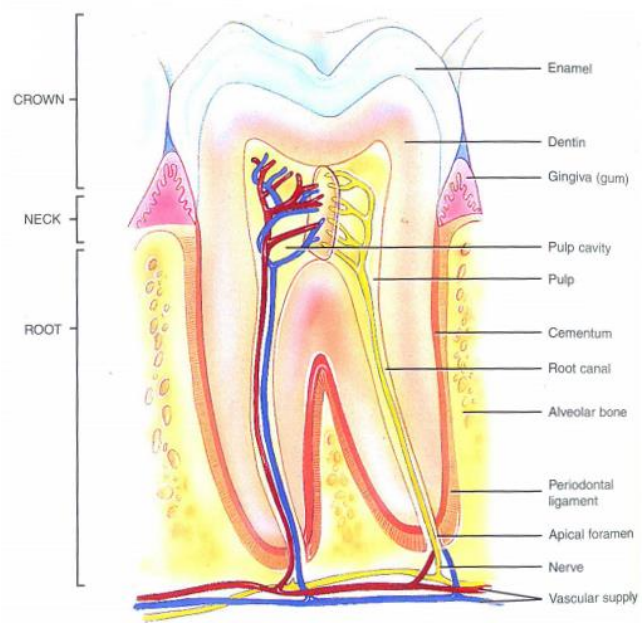

Figure 3. The anatomy of a tooth *(14)*. On the left hand side of the structure three main components of a tooth is presented, the crown, neck and root. On the right hand side the structural components of a tooth is shown in detail, such as the enamel and the dentin making up the crown.

For a natural tooth the root is not anchored directly into the jawbone, instead it is anchored to the root cementum and the periodontal ligament. This is made up by a dense fibrous connective tissue substance, similar to the fibrous connective tissue surrounding the neck, see Figure 1 (5). The root cementum and the periodontal ligament encloses the root and anchors the tooth to the bone, it also helps absorb mechanical stimulus during chewing (14).

2.2. Dental abutments

The dental abutment is the middle part of the dental implant, see Figure 1, and can structurally and functionally be compared to the neck of a tooth, see Figure 3. The abutment interacts with the peri-implant mucosa, and is thus in contact with soft tissue. The interaction between the abutment and the peri-implant mucosa is important for the long term success of a dental implant (9). The abutment must be able to provide a surface structure that compositionally and structurally enables adhesion to the different components of the peri-implant mucosa. The peri-implant mucosa is made up by a collagen rich tissue, containing human gingival fibroblasts, and a layer of junctional epithelium rich in epithelial cells. Preferably, the abutment surface should disfavor adhesion of bacteria to its' surface. These properties place very specific requirements on the abutment surface characteristics. It is also believed that a part of the key to a long-term clinical and esthetical successful implant lies in optimizing the abutment's surface characteristics, and thus the surrounding soft tissue profile (15).

2.2.1. Composition of peri-implant mucosa

The main structural differences between peri-implant mucosa and gingiva is the perpendicular fibers seen in gingiva surrounding a tooth, see Figure 2. These fibers are absent in peri-implant mucosa, weakening the barrier between the internal of the body and the external oral cavity (5). Gingiva and peri-implant mucosa also differ in terms of composition (16). The compositional differences, as well as the structural differences, are a consequence of the surgical procedure of placing the implant (5).

Peri-implant mucosa can to some extent be compared to scar tissue, as it contains a lot of collagen and keratinized mucosa compared to gingival tissue (10). Peri-implant mucosa contains 85% collagen compared to 65% for gingival tissue. The peri-implant mucosa has also been observed to have fewer blood vessels, and can therefore support fewer cells (17). Normal gingival tissue contains about 15 % fibroblasts, and the number of fibroblasts observed around titanium implants is approximately 3 % (17). The low amount of cells surrounding titanium implants can be explained by the lack of periodontal ligament, since the periodontal ligament provides a fine network of small blood vessels capable of supporting a higher number of cells. The lower density of blood vessels in the peri-implant tissue can be considered to reduce the immune response in the peri-implant tissue (17).

2.2.2. Apical migration

Apical migration is a phenomenon observed when the peri-implant tissue around an implant starts to retract, leaving part of the abutment visible. This phenomenon has clinical as well as esthetic disadvantages (8). During insertion of a bone anchored implant some extent of apical migration is unavoidable. This is because upon insertion of the implant a healing process is initiated. During this process salivary glands excrete an epidermal growth factor (EGF) which stimulates growth, migration and proliferation of fibroblasts and epithelial cells (18). However, some observations state that the presence of EGF also induces bone resorption (5). During the healing process the concentration of EGF in the soft tissue is high. This also causes the EGF concentration at the bone-soft tissue interface to be higher than normal, which induces bone resorption around the collar of the screw, see Figure 4A. When the soft tissue growth surrounding the abutment is finished and the wound has healed, the levels of EGF decrease and the bone resorption will stop, see Figure 4B. However, the bone resorption results in a hollowing in the bone surrounding the implant and causes some apical migration of the soft tissue surrounding the abutment to be visible (5).

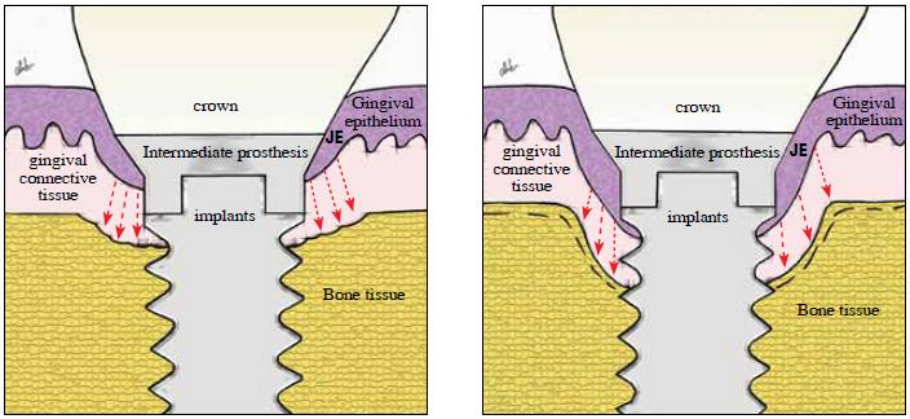

Figure 4. Scheme of the bone resorption observed surrounding dental implants. A. Shows the different tissue layers upon insertion of a dental implant. B. Visualizes the different tissue layers when bone resorption has stopped. (5)

2.3. Cell adhesion

Long term success of a dental implant is dependent on a good contact between the abutment and the soft tissue. A strong adhesion of soft tissue to the abutment surface is dependent on the physical and chemical properties of the abutment surface (19).

Immediately upon insertion of a biomaterial in the body the surface is immersed in bodily fluids and a layer of ions is absorbed onto the surface. The composition of the adsorbed layer largely depends on the surface charge and wettability properties of the abutment surface. Following the adsorption of ions, proteins from saliva and blood is adsorbed onto the surface (4). The adsorption of molecules onto the abutment surface enables cellular interactions. Cells are not able to bind straight to the abutment surface, but can bind to a number of proteins absorbed onto the surface. Fibrin and fibrinogen are two examples of proteins related to cell adhesion (20).

The mechanism of cell adhesion is through transmembrane proteins called integrins, which bind to the cytoskeleton within the cell. All human kinds of integrins are known to bind to talin inside the cell. The integrin is then connected to the cytoskeleton, see Figure 5. In epithelia cell-matrix adhesion sites are called hemidesmosomes, which is a special kind of integrin binding to keratin filaments. Fibroblasts are capable of creating strong permanent adhesion points to surfaces via so called focal adhesions, which can be identified by presence of vinculin, another actin binding protein.

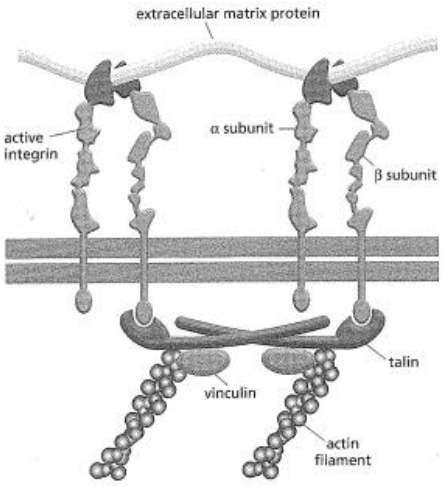

Figure 5. Integrins are transmembrane proteins which mediate cell adhesion. The protein is a dimer, made up by two subunits, α and β. Inside the cell, the integrins are anchored to actin filaments and the cytoskeleton via talin and vinculin. On the outside of the cell the integrins can bind to extracellular matrix proteins such as fibrin and fibrinogen.

Evaluation of the number of adhesion points, hemidesmosomes and focal adhesion, indicates the strength of the soft tissue contact between the abutment and the peri-implant mucosa. The more adhesion points present, the better the adhesion, and the better the soft tissue contact.

2.3.1. Influence of surface characteristics on cell adhesion

Designing an abutment with a coating that promotes good soft tissue contact could potentially shorten the healing time for patients undergoing dental implant treatment. This, reducing the risk for infections, and provide esthetic advantages for the patients by preventing apical migration (19).

As mentioned in the previous section the abutment adsorbs ions and proteins upon immersion in bodily fluids. The composition of the adsorbed layer is largely determined by the chemical composition and the hydrophilicity of the abutment surface (4). Important proteins for cell adhesion, such as fibrinogen adsorb more readily on hydrophilic surfaces (21). Consequently, it has been observed that fibroblasts and epithelial cells adhere and spread better on hydrophilic surfaces as compared to hydrophobic surfaces (4).

The roughness of the abutment surface can also affect the adsorption of proteins, by affecting the orientation of the molecules adsorbed onto the surface. The orientation of an adsorbed protein can either hide or expose cellular receptors, such as integrins, which are responsible for cell adhesion. For example fibrinogen, an important protein for cell adhesion, adsorb much readily on smooth surfaces compared to rough surfaces (4). This complies with stronger adhesion and more spreading of epithelial cells and fibroblasts on smooth polished titanium surfaces compared to rougher titanium surfaces. Studies show that these two cell types prefer a hydrophilic smooth finely grooved titanium surface for adhesion and proliferation (22) (23).

2.4. Biofilm formation

Surgical insertion of a dental implant into the body is far from sterile, and the oral cavity is rich in bacteria. Formation of a biofilm on the abutment surface may cause an infection, and thus require further medical treatment (13). Formation of a biofilm between the implant and bodily tissues, for example between the abutment surface and the peri-implant mucosa, can in worst case require a removal of the entire implant (13). This is because biofilms are difficult to treat.

Biofilms are bacterial multicellular communities enclosed by extracellular matrix that bacteria produce themselves (11). The high resistivity to microbial agents such as antibiotics can be derived from their extracellular matrix. The matrix acts as a diffusion barrier to molecules trying to penetrate the biofilm. This is the reason why biofilms are hard to treat and sometimes lead to chronic infections (11).

Biofilm formation can occur on implant surfaces in contact with both hard- and soft tissues. However, the location of the soft tissue (next to the oral cavity) makes it more susceptible for bacterial infection compared to the underlying bone tissue (13). Biofilm formation has been closely related to the surface topography (12). By preventing bacteria to adhere or reducing the amount of bacteria in the peri-implant mucosa, the formation of biofilm can be counteracted. And can potentially reduce the risk of hard-to-treat infections (24).

2.5. Antibacterial surface coating

As discussed in previous sections the surface's chemical composition determines its' properties in terms of hydrophilicity and surface charge (4) In addition to modifying the surface properties to improve the soft tissue contact, surface coatings can be used to reduce the adhesion or presence of bacteria (12). As mentioned in the introduction, there are two different main approaches to designing antibacterial surfaces. The first approach is to incorporate toxins or antibiotics into the surface coating, and the second is to reduce the amount of bacteria which attach to the surface.

The aim of antibacterial coatings is to reduce the amount of bacteria present in the peri-implant mucosa. For example, preventing biofilm formation may improve the ability of the peri-implant tissue to achieve proper soft tissue contact. It has been observed that the presence of bacteria on the abutment surface, delays the formation of soft tissue contact (4). By avoiding the formation of a biofilm, the healing time could potentially be shortened, as well as the chance of long-term clinical success would increase significantly (8).

Material characteristics such as high resistance to corrosion and wear have made TiN suitable for coatings of medical tools (25). Studies have shown that abutments coated with TiN have indicated reduced amount of bacteria adhering to the abutment surface (12). Evaluation of TiN coatings with *in vitro* and *in vivo* models have not shown a negative effect on the adhering and spreading abilities of fibroblasts and epithelial cells (6) (4). These results support that TiN-coatings are compatible with peri-implant mucosa, and can provide a good soft tissue contact.

2.6. Surface deposition techniques

Surface deposition techniques are useful in surface engineering. For example, the surface's morphology, wettability and composition can be altered using these techniques. When introducing new components and molecules to a surface, the surface composition will be different from the composition of the bulk, creating a new surface layer (26). There are some limitations of what surfaces layers can be applied to a material. The deposited surface layer needs to adhere to the underlying material. Without attractive forces between the surface layer and the bulk there will be separation between the two. These attractive forces can be of different nature, for example it could be electrostatic forces, mechanical retention or covalent chemical bonding (26).

2.6.1. Physical Vapor Deposition

The set-up of physical vapor deposition, PVD, is a low-pressure chamber, with an inert- and a reactive gas feed. The substrate to be coated is located inside the chamber, see Figure 6 (26). During the process the pressure in the gas containing chamber is reduced to about 4 % of the atmospheric pressure. The low pressure causes dissociation of the reactive gas as well as the formation of argon

ions, creating a plasma (27). The argon ions are bombarded towards the substrate, forming ions on the surface, which react with the surrounding reactive gas, forming a coating. By controlling the bombardment of the substrate the surface topography can be modified (26).

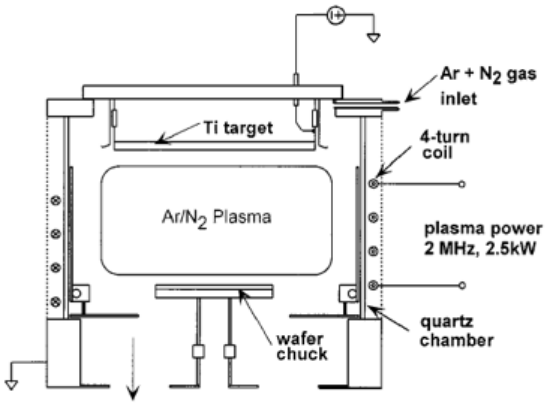

Figure 6. Simplified model of a PVD set-up. (27) The Ar and N_2 gas is fed into the chamber through the inlet. The plasma dissociates the N_2 gas and causes the Ar particles for form ions. The Ar ions is then bombarded onto the surface to create Ti+ ions on the surface. These can then react with the dissociated nitrogen to form a TiN coating on the substrate, in this case titanium. (26)

For abutments to be coated with TiN, nitrogen gas is used as the reactive gas phase, and titanium as the substrate. For the inert gas phase most commonly argon is used (26). During the process nitrogen reacts with titanium ions formed on the surface and a layer of TiN is formed on the underlying titanium. This technique is usually used for formation of thin layers, suitable for application on dental abutments.

2.7. Analytical Techniques

For assessment of cellular response as well as surface characteristics of different coatings a number of analytical techniques can be useful. For evaluating cellular response fluorescent microscopy and fluorescent probes can be useful (20). For surface characteristics contact angle measurements and profilometry are useful. Scanning Electron Microscopy (SEM) can be used for visualization of cells, as well as for visualization of the micro- and submicrostructure.

2.7.1. Scanning Electron Microscopy (SEM)

Scanning electron microscopy (SEM) is one of the most versatile methods for analyzing surface structures in 3D. It works similarly to a light microscope but the light source has been replaced with an electron beam. The short wavelengths of electrons compared to light enable this technique to generate high-resolution images down to 1 nm (28). Due to the energy source being electrons, a vacuum chamber is needed, as any particles present could interfere with the imaging.

In order to produce higher resolution images the electron beam passes through a series of lenses prior to reaching the sample, see Figure 7 (28). The lenses collect the beam and thereby reduce the sample area hit, enabling higher resolution images to be obtained (28). For samples to be analyzed using SEM the surfaces have to be conductive. For non-conductive materials a conductive layer is usually applied. Cell samples are usually sputtered with gold prior to analysis.

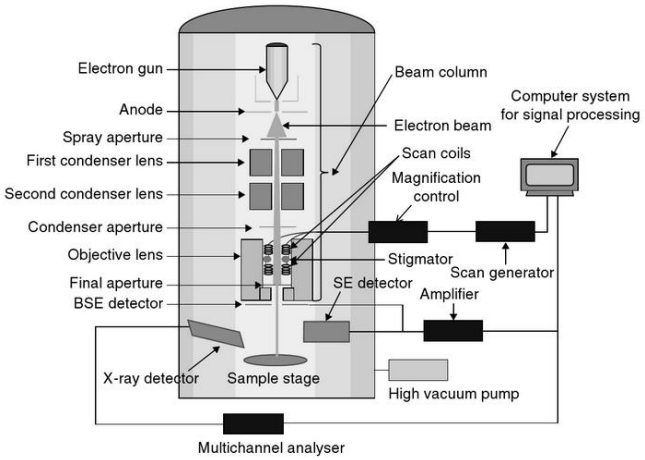

Figure 7. Schematic view of the SEM set-up (28). The sample is placed in a vacuum chamber and bombarded by an electron beam. Reflected electrons are collected by a number of detectors and analyzed to give information about the samples morphology, phase and chemical composition.

The conductive layer is needed as the detectors collect reflected electrons from the beam-sample interaction. Both reflected electrons from the beam and electrons which have escaped from the surface are needed for analyzing the sample. These electrons are called backscattered electrons and give information about the chemical composition of the sample. A variety of electrons are reflected from the beam-sample interaction, these are amplified and processed to give a real-time image during the analysis. Together these signals provide information about the substrates morphology, phase and chemical composition (28).

2.7.2. Contact Angle Measurements

A simple way to interpret a surface's wettability and surface energy is by contact angle measurements. The technique measures the angle of the tangent line at the base of a liquid droplet resting on a solid surface, this angle is the contact angle, θ (°), see Figure 8 (29).

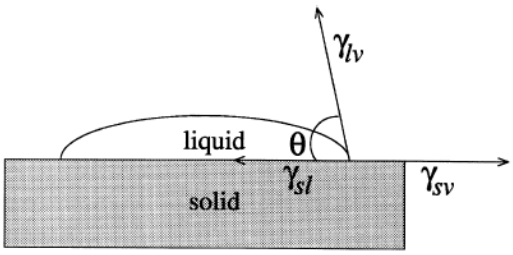

Figure 8. Image of a sessile droplet. (29) The tangent on the droplet at the intersection between liquid and solid is a measurement of the contact angle.

The droplet resting on the solid surface is in equilibrium in between three interfacial tensions: solid-vapor, γ_{sv} , solid-liquid, γ_{sl} , and liquid-vapor, γ_{lv} (29). The equilibrium between these interfacial tensions is been described by Young's equation:

$$\gamma_{lv} \cos \theta_Y = \gamma_{sv} - \gamma_{sl} \quad (29)$$

This equilibrium works well on inert, chemically homogeneous and smooth surfaces. Most surfaces are not completely homogeneous chemically or structurally, and hysteresis of the droplet is observed. Measuring contact angles on these surfaces reflects the surfaces topography rather than the solid-liquid tension, γ_{sl} (29).

For this study the effect of roughness as well as chemical heterogeneity on the contact angle is of less importance compared to the measured contact angle, as this is the wettability experienced by the cells during the experiments (29). These factors would be significant if aiming to accurately determine the solid-liquid interfacial tension.

2.7.3. Profilometry

A profilometer is a stylus instrument, and it is used for measuring surface roughness. Measurements are performed by moving a sharp probe, a stylus, in a straight line across the surface of a sample, and amplifying the signal to a useful level. A data analyzer records and processes the data from the measurement and generates a few parameters used to characterize the surface roughness (30).

When characterizing the 2D roughness of a surface mainly vertical alternations are considered. However, for a proper characterization of the surface it is also relevant to consider the average horizontal distance between the vertical peaks (30). However, for basic surface characterization only the vertical alternations are considered (30). These vertical alternations are described by a parameter R_a (31). R_a serves as an average surface roughness parameter, and gives an average of the absolute vertical variations along the straight sample line (31). When designing the experimental setup for profilometry measurements it is important to cover as many areas of the sample area as possible, such as the middle and the sides of the sample.

1.1.1. Fluorescence Microscopy

Fluorescence microscopy is light microscopy which can be used for visualization of different structure of the cells. Prior to analysis the sample is pretreated with a molecule attached to a fluorescent probe (20). This molecule acts as a vector and binds to a specific structure or protein within the sample cells. A fluorescent probe absorbs light at a specific wavelength and emits at another enabling visualization of this specific structures (20).

When observing the sample in the fluorescence microscopy the sample is exposed to a beam of light. The light beam interacts with the sample and is collected by an objective lens, and the beam finally passes through an emission filter before reaching the eyepiece, Figure 9 (32). The emission filter is related to the fluorescent probe used, it only allows light of the wavelength emitted by the fluorescent probe to reach to eyepiece. This enables high resolution visualization of structures or proteins within the cell.

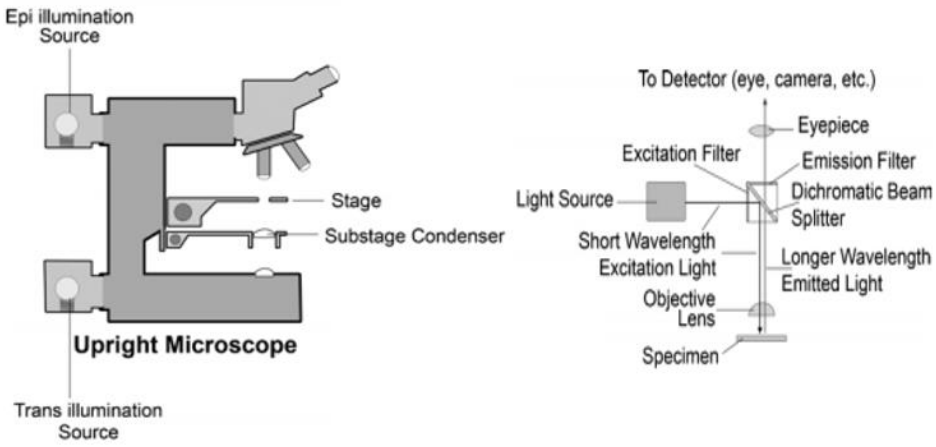

Figure 9. Schematic image of a fluorescent microscopy (32).

Examples of fluorescent probes are phalloidin and DAPI. Phalloidin binds and fixates f-actin and hence visualizes the cytoskeleton of cells (33). This is useful when aiming to evaluate a cell's

morphology and proliferation. DAPI on the other hand binds to A-T rich domains of double stranded DNA (34). For living cells DAPI serves as a useful probe for visualization of the nucleus.

2. Materials and Methods

The materials and methods used in this study is presented and explained in this section.

2.1. Specimens

A total of 43 circular discs (Ø: 6,25 mm, thickness 2 mm) of commercially pure (cp) titanium Ti (grade 4) were included in the study. The specimens were cleaned and dried in ambient temperature. They were then divided into four different groups, of which one served as control (Ti) and was not subjected to further surface treatment. Using Physical Vapour Deposition (PVD) titanium nitride (TiN) and chemically modified TiN (TiN_1 and TiN_2) were deposited on the other groups. After deposition of coatings, the specimens were packaged in plastic containers and sterilized with electron beam irradiation.

2.2. Surface characterization

Methods for surface characterization are presented in the following sections.

2.2.1. Scanning Electron Microscopy (SEM)

Surface morphology was analyzed with Environmental Scanning Electron Microscopy (XL30 ESEM, Philips, Netherlands) at an acceleration voltage at 10 kV for SEM analysis. A magnification of 500 times was used.

2.2.2. Contact angle measurements

A contact angle measuring system (Drop Shape Analysis Systems DSA 100, Kruss GmbH, Germany) was used for contact angle measurements. For each sample group three coins were evaluated.

A droplet of 10 µl deionized water was placed on top of the metallic coin. A microscopy was used to take a picture of the droplet once it was placed on the surface. A computer software was used to calculate the contact angle for each droplet, see Figure 10. Two droplets per coins were measured.

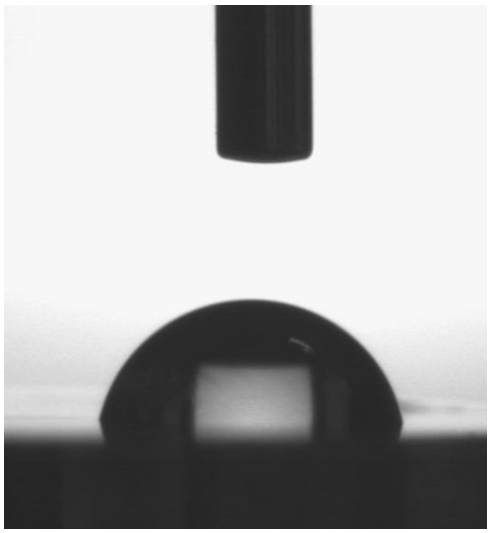

Figure 10. Image from the contact angle measurement. The contact angle was calculated as described in section 2.7.2.

2.2.3. 2D Stylus Profilometry

The surface roughness was measured with a 2D Stylus Profilometry (Hommel T1000 wave, Hommelwerke GmbH, Germany). A vertical measuring range of 320 µm and an assessment length of 4,8 mm were used. The profilometer was set to measure a distance of 4,8 mm with a cut off of 0,8 mm on each side, consistent with ISO 11562. The surface roughness in terms of arithmetic mean

value of vertical deviations of the roughness profile from a mean line (R_a) was calculated using a filtering process.

Three coins per sample groups were measured with three measurements per coin according to Figure 11.

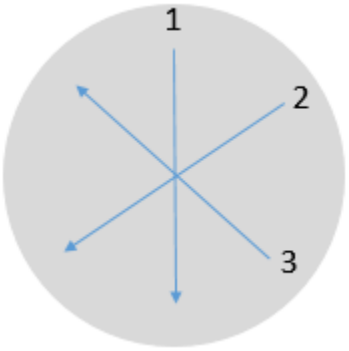

Figure 11. 2D Stylus profilometry measurements were performed three times on each coin as shown in figure.

2.3. Cell culture and cell staining

For the cell studies two different cell lines were used and evaluated, initially fibroblasts from mouse, 3T3, and later also human gingival fibroblasts (HGF-1). These were treated in the same way, with reservation for the cultivation time, as HGF-1 cells needed longer time to reach confluence.

Throughout the study cells were grown on different titanium coins. For visualization of the cells fixation and fluorescent probes was necessary. This was due to the available light microscope having the light source located below the sample holder and no light could penetrate the metallic coin. For sequential studies over time, multiple samples were prepared and fixated at different times during the experiment. The experiments were repeated to confirm that trends observed during experiments were consistent.

2.3.1. Cell culturing and seeding of cells on metallic coin

For cell culture Dulbecco's Modified Eagle Medium (DMEM) with addition of 10 % fetal calf serum and 1 % penicillin was used for both cell lines. Cells were cultured at 37 ˚C and 5 % CO_2.

Splitting of cells

3T3 cells were split 1/10 twice a week, HGF-1 cells were split 1/3 once every week. The culture flask to be split was removed from the incubator and placed in a sterile fume hood. The old medium was decanted from the culture flask. Cells were rinsed once, using versen, a salt solution. Rinsing of cells was done by adding versen to the flask, shaking it, and decanting the liquid. Cells were dissociated from the bottom of the culture flask by adding a trypsin solution, 2,5 % trypsin in versen. The culture flasks were then placed back into the incubator for a few minutes.

A light microscope was used to verify that all cells had dissociated from the bottom of the culture flask. When dissociation of cells could be verified, new medium was added to the culture flask and the content was mixed thoroughly by pipetting the liquid up and down. A new culture flask was prepared by adding new medium to it. Finally cell solution from the old culture flask was transferred to the newly prepared one. How much cell solution was taken depended on the splitting ratio, see above.

Seeding of cells on metallic coins

For seeding of cells on the metallic coins, cells were dissociated from the culture flasks as described in the section above. However, the cell solution from the old flask was transferred to a tube of new medium instead of to a new flask. This tube was mixed thoroughly prior to seeding.

The metallic coins were prepared by placing the coins in a 24-well plate, one coin in each well. Once ready for seeding a droplet of the cell solution, 45 µl, was placed on top of each coin. The 24-well plate containing the coins was then placed into the incubator set to 37 ˚C and 5 % CO_2 for 1 hour. After 1 h, 1 ml of growth medium was added to each coin containing well.

2.3.2. Cell staining with phalloidin and DAPI

Upon removing the cell samples from the incubator, the growth medium was removed, and cells were washed twice with PBS heated to 37 ˚C. For fixation cells were immersed in a 37 ˚C fixating solution for 10 minutes, 4 % formaldehyde in PBS for green phalloidin and 2,5 % glutaraldehyde in PBS for red phalloidin. Coins were then washed another three times using PBS. Cells were permeabilized by immersing them in 0,2% Triton X100 in PBS for 15 minutes. From this stage on, samples were kept dark. Coins were finally washed twice in PBS, and kept in PBS at 4 ˚C until staining with phalloidin or DAPI (maximum two days after fixation).

Upon staining with phalloidin, the coins were removed from the 24-well plate and placed on a piece of parafilm, cell-side facing up. A droplet of block solution (20% fetal bovine serum in PBS), 45 µl, was placed on top of the cells for 30 minutes, see Figure 12. The cells were washed twice with PBS. Washing at this stage was done by removing the existing droplet by gently touching the side of the coin with a piece of tissue. Then a new droplet with PBS was added, left for a few minutes before removing the droplet in the same way. For staining of actin a droplet of phalloidin, 45 µl, was placed on top of the cells. The droplet was removed after 20 minutes. Cells were washed another three times with PBS and finally once with deionized water.

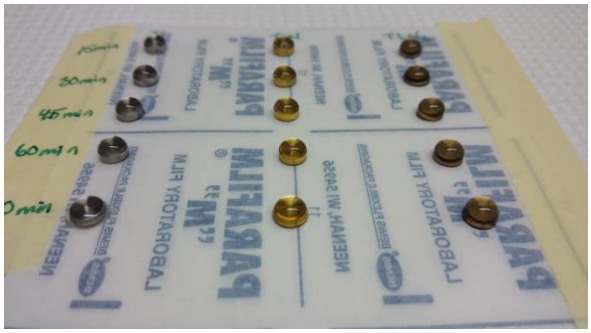

Figure 12. Image shows coins which are being prepared for staining with phalloidin. Three rows with the three different sample groups are seen. From left: Ti, TiN and TiN_2. On top of each coin is a droplet of block solution.

Finally the coins were mounted onto microscopy slides by placing a droplet of prolong gold on the microscopy slide. The coin was placed with the cells facing up on the droplet. For staining with DAPI, prolong gold with DAPI was placed on top of the cells and finally a coverslip was mounted on top of the droplet, see Figure 13. Microscope slides were left to set in room temperature, however, they were still kept dark. Prior to examining the coins in a fluorescent microscopy the top of the cover slip was gently wiped with ethanol.

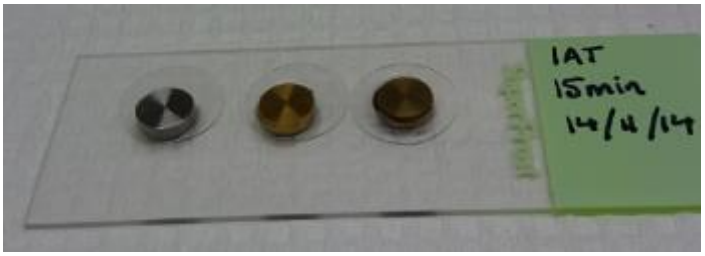

Figure 13. Image shows the mounting of coins onto microscopic slides. On top of the cells a droplet of prolong gold with DAPI is places. Cover glasses are places on top of each sample.

2.4. In vitro cellular response

Methods for evaluation of *in vitro* cellular response are presented in the sections below.

2.4.1. Visualization of cell morphology using SEM

For preparation of SEM analysis, cells on titanium coins were prepared according to the following procedure. Upon removing the samples from the incubator (one day after seeding), cells were fixated with 2,5% glutaraldehyde in H_2O for 10 minutes. Samples were kept in the 24-well plates and rinsed carefully with PBS. Samples were then post fixated by placing a 45 µl droplet of 1% OsO_4/ (PBS diluted with to 2/3 with H_2O) for 1 – 4 h at +4 ˚C on top of the cells. Samples were rinsed with distilled water for at least 15 minutes upon a droplet of 45 µl 1 % thiocarbohydrazide, TCH, was placed on top of the coins for 10 minutes in room temperature. The THC solution had to be freshly made and filtered before use. Samples were rinsed with distilled water for 15 minutes.

The samples were treated once again with OsO_4 for 60 minutes, washed and treated with THC for 15 minutes, and finally with OsO_4 for 30 minutes and rinsed in distilled water.

Samples were then kept in distilled water until the day of SEM evaluation. On the day of SEM analysis, the samples were dehydrated through an ethanol series (see below) and finally dried with hexamethyldisilazane (HMDS) 2-3 times for 5-10 minutes each. Samples were left to dry in fume hood for at least 1,5 h.

Ethanol dehydration series:

- 70 % ethanol 2 x 5-10 minutes
- 85 % ethanol 5-10 minutes
- 95 % ethanol 5-10 minutes
- 100% ethanol 4 x 5-10 minutes

Finally samples were sputtered with gold using a sputtering machine (Sputter coated 180 auto, Cressington Scientific Instrument, England).

2.4.2. Growth study

Results from the growth study aimed to evaluate cell survival and growth on the four different surfaces over a five day period. Five coins from each sample group were seeded with cells as described in section 2.3.1, and placed in the incubator, 37 ˚C. Upon 24 h of cell growth one coin from each sample group was fixated and stained with phalloidin and DAPI. The samples were analyzed in terms of the number of cells on each surface, cells were counted using fluorescent microscopy. The analysis area was 6 mm^2. One coin from each sample group was fixated and analyzed every 24 h over a 5 day period.

2.4.3. Initial adhesion test

For the initial cell adhesion test the cells were seeded as described in section 2.3.1. However, as the study was performed over a time period of 90 minutes, no growth medium was added one hour after seeding. Upon seeding cell solution, one coin from each sample group was rinsed and fixated every fifteen minutes, upon staining with DAPI, see Figure 14.

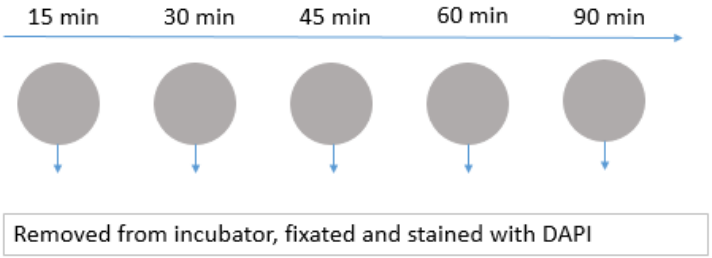

Figure 14. Experimental setup for the initial adhesion test.

The initial adhesion study was evaluated by studying the number of adhered cells for each coin using a fluorescent microscopy. One image was taken of the coin using five times magnification, see Figure 15. A marking tool in Photoshop was used for calculations of the number of cells.

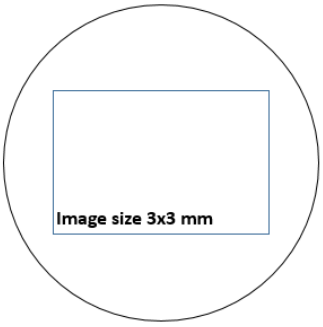

Figure 15. Describes the images taken of each coin during initial adhesion studies. Cells within the image were calculated using a marking tool in Photoshop.

2.4.4. Wound healing Assay

Five coins from each sample group were seeded as described in section 2.3.1, and placed in the incubator. Experiments started when samples reached confluence, approximately 3 days from seeding for HGF-1 cells and two days for 3T3 cells. In order to stimulate a wound, each coin was scratched using a pipette tip (20-200 µl). To remove any excess debris coins were washed twice in growth medium (35).

One coin from each sample group was fixated instantly whereas the rest of the samples were placed in the incubator at 37 ˚C at 5 % CO_2. Counting the time of scratching as the starting point of the experiment, one coin from each sample group was fixated every second hour. Including the coin fixated at the start of the experiment, coins were fixated at the following times: 0h, 2h, 4h, 6h and 8h, see Figure 16.

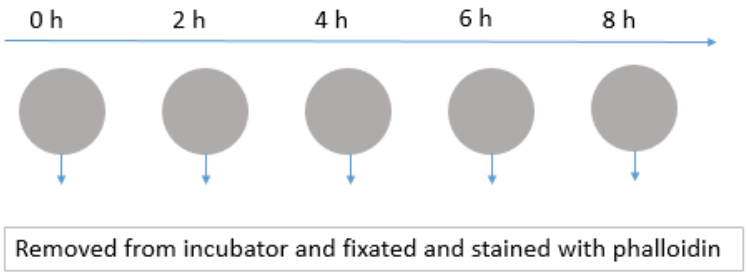

Figure 16. The experimental setup for one sample group during wound healing assays.

For evaluation of the wound healing experiment all coins fixated during the experiment were stained with phalloidin and DAPI. Using fluorescent microscopy and several images taken at ten times magnification along the "wound", the samples could then be evaluated by measuring the gap distance over time. As the total gap distance can vary within the same wound as well as from coin to coin, only measuring the gap distance after a specific time does not give a comparable measurement of the wound healing process. To get a more reliable measure, the gap distance after a specific time, d_t, was divided with the gap distance at time zero, d_0, using equation [1], see Figure 17. This gives a value of the percentage of the wound which has not healed.

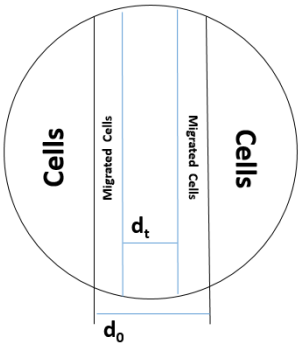

Figure 17. Gap distances measured during the evaluation of the wound healing assay. The two distances measured represents the gap distance at the beginning of the experiment d_0, and the distance remaining after a specific time d_t.

$$X = 1 - \frac{d_t}{d_0} \qquad (1)$$

The value of X represents the percentage of the wound which has healed due to migration of cells during the experiment. The gap distances were measured using the measuring tool in *Photoshop PS* and then converted into µm.

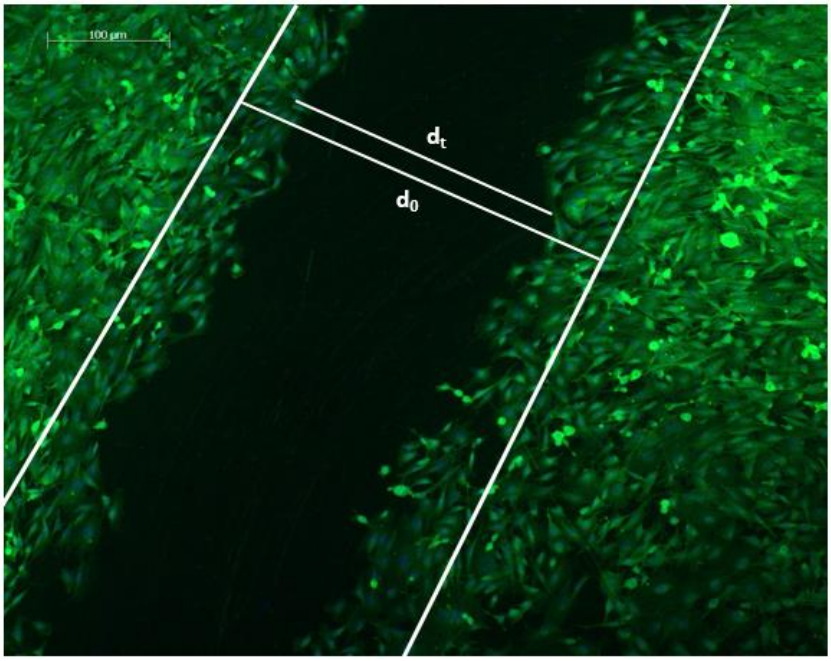

Figure 18. An example of an image taken during a wound healing experiment, this image is from 3T3 cells grown on TiN-samples for six hours. The image illustrates how d_t and d_0 were measured to calculate the percentage of wound healing for the samples.

Each coin was photographed twice to cover most of the artificial wound. The gap distance was measured at three points on each image, giving a total of six measuring points per sample, see Figure 18.

3. Results

Characterization of the four different sample groups was performed using SEM, contact angle measurements, and 2D stylus profilometry. The cell studies, aimed to determine the cell viability, proliferation and migration on the different surface coatings. Originally three different surfaces were investigated: Ti, TiN and TiN_2. Later in the project a fourth surface was included, TiN_1.

3.1. Scanning Electron Microscopy (SEM)

From Figure 19 it can be seen that all coins have spherical marks (machining tracks) from the production process, it can also be seen that TiN_1 and TiN_2 samples have a more heterogeneous surface structure as compared to Ti and TiN samples.

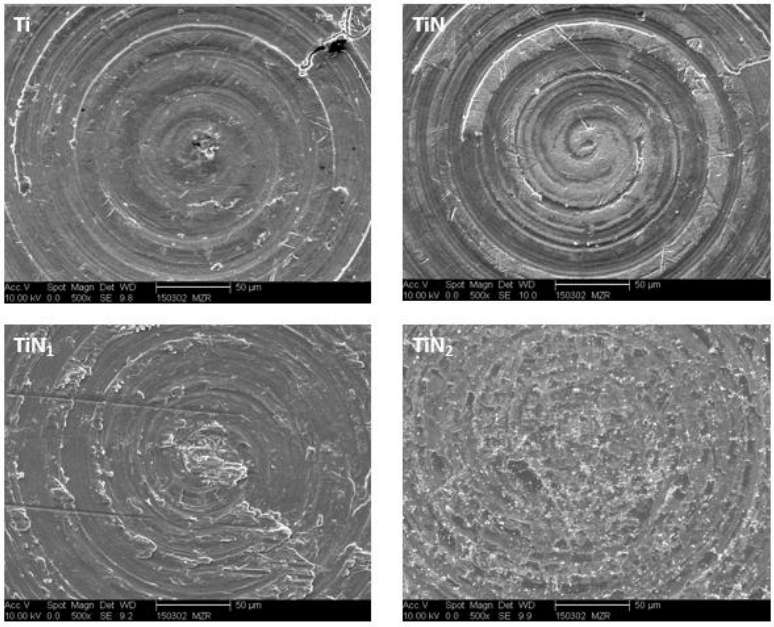

Figure 19. Images from SEM analysis of the four different sample groups used in this study.

3.2. Contact Angle Measurements

Contact angle measurements were performed on all four surfaces. The surface modifications performed increased the hydrophobicity of the surface in the following order: Ti < TiN < TiN_1 < TiN_2, see Table 1.

Table 1. Results from contact angle measurements using the sessile drop method.

Sample	Average Contact angle (˚)	St. Dev (˚)
Ti	79,2	1,9
TiN	86,5	5,2
TiN_1	100,9	2,8
TiN_2	115,9	3,4

3.3. 2D Stylus Profilometry

Results from the 2D Stylus Profilometry is presented in Table 2 and shows that the surface roughness is very similar for all samples but the TiN_1-coatings, which have a higher surface roughness, in term of a higher R_a value.

Table 2. Results from the 2D Stylus Profilometry measurements.

Sample	R_a (Average Surface Roughness (µm))	St. Dev (µm)
Ti	0,14	0,01
TiN	0,14	0,01
TiN_1	0,24	0,01
TiN_2	0,14	0,02

3.4. *In vitro* cellular response

The results from the *in vitro* cell studies are presented in the sections below.

3.4.1. Visualization of cell morphology using SEM

Images from SEM analysis of both 3T3 cells and HGF-1 cells are presented below. Images represent cells one day after cell seeding.

HGF-1 Cells

SEM-analysis of Ti-samples shows a few very long cells, see Figure 20. However, no cells are seen on TiN or TiN_2 samples.

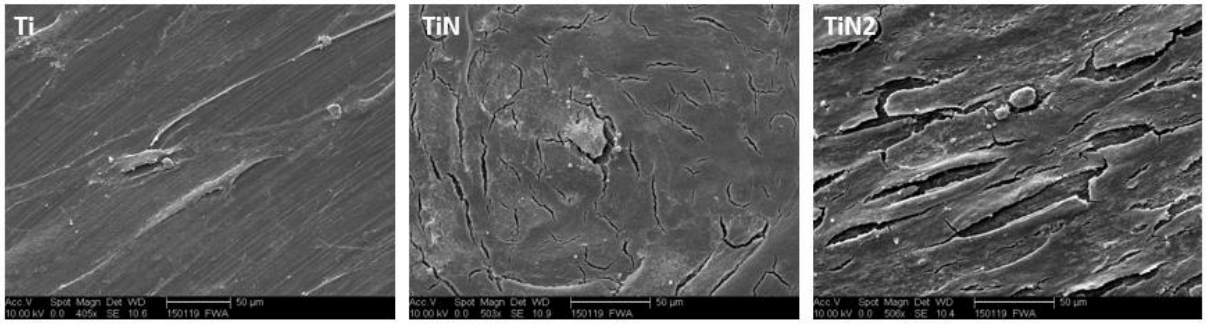

Figure 20. SEM analysis of HGF-1 cells on TI, TiN and TiN_2 samples at 500 times magnifications.

3T3 Cells

SEM analysis of 3T3 cells shows that 3T3 cells have a round morphology on all three surfaces.

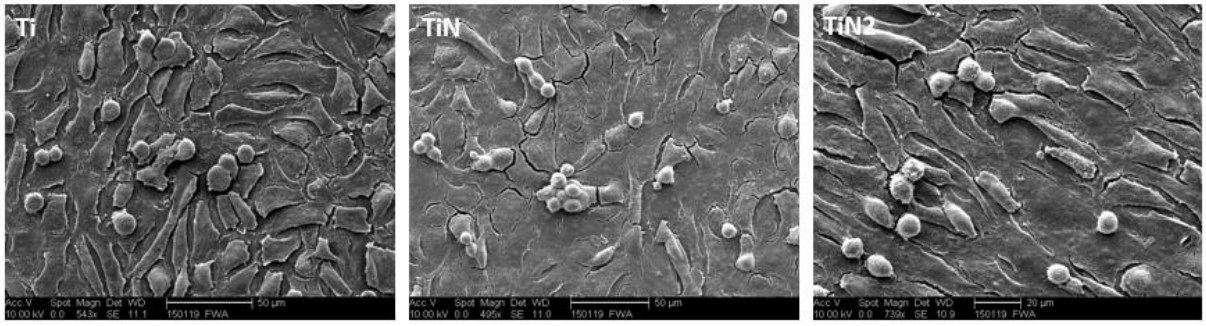

Figure 21. SEM analysis of Ti, TIN and TiN_2 samples at 500 times magnifications.

3.4.2. Growth study

Images in Figure 22 shows the result from growth study. It can be seen that cell growth on TiN and TiN_1 samples is comparable to cell growth on uncoated Ti-samples. Cell growth is not supported by TiN_2-samples.

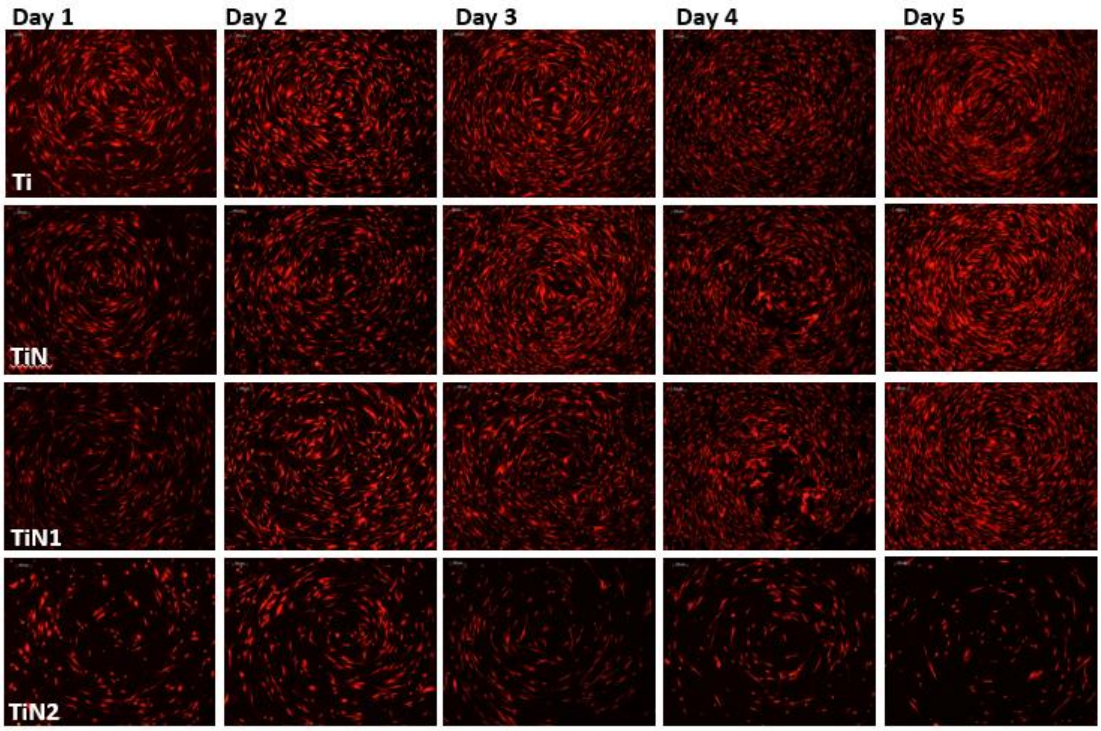

Figure 22. Images of the four different sample surfaces included in the growth study the first five days.

Based on the images in Figure 22 the number of cells in each image is presented graphically in Figure 23, for all values see appendix A.

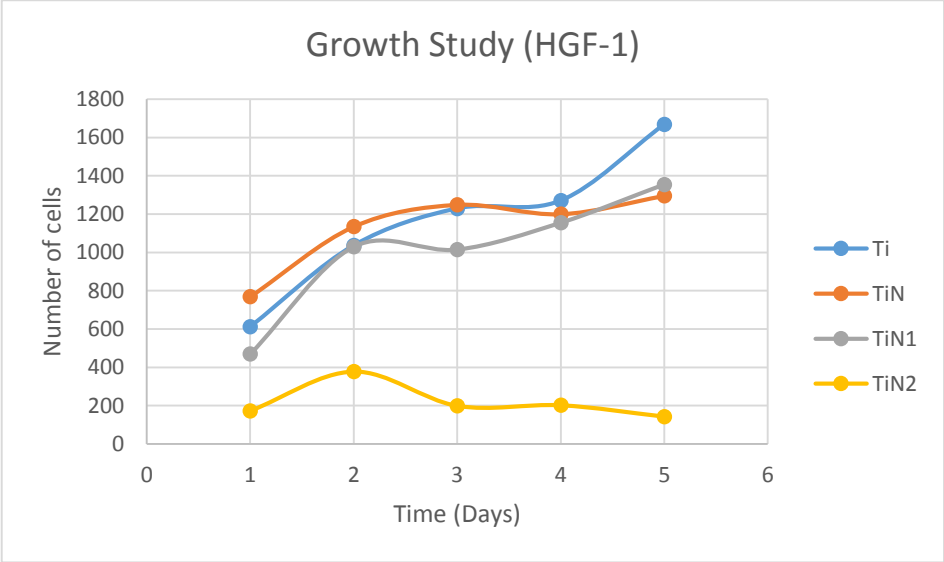

Figure 23. Graphical representation of the growth study performed with HGF-1 cells over a five day period. Graph shown that TiN_2-samples are unable to support cell growth during this time frame.

3.4.3. Initial cell adhesion

Initial cell adhesion studies were performed to evaluate the coating effect on the initial adhesion potential of both 3T3 cells and HGF-1 cells. Values from initial adhesion studies for both 3T3 cells and HGF-1 cells can be found in appendix B

HGF-1 Cells

Results from the initial adhesion studies over the first 90 minutes upon cell seeding show no difference, Figure 24.

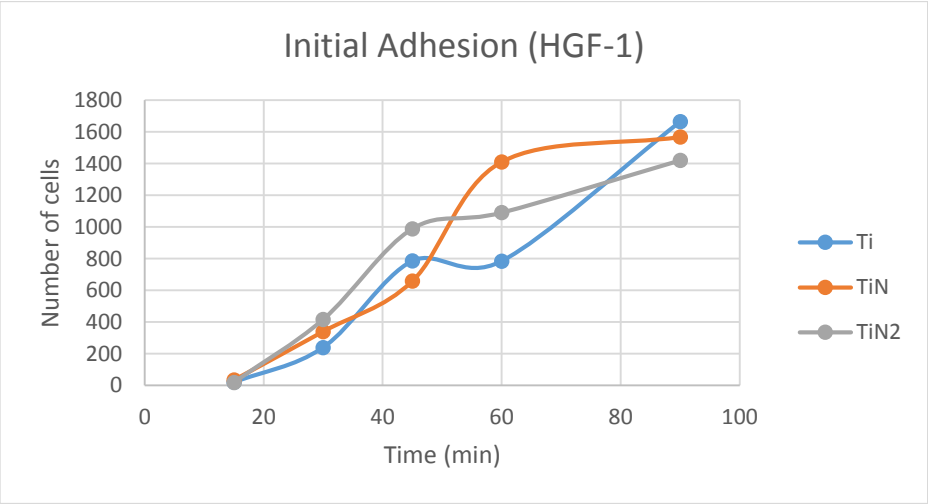

Figure 24. Results from initial adhesion studies with HGF-1 cells.

3T3 cells

Results from initial adhesion tests for 3T3 cells are shown in Figure 25. No difference in the initial adhesion during the initial 90 minutes is seen for 3T3-cells can be seen for Ti, TiN and TiN_2-samples.

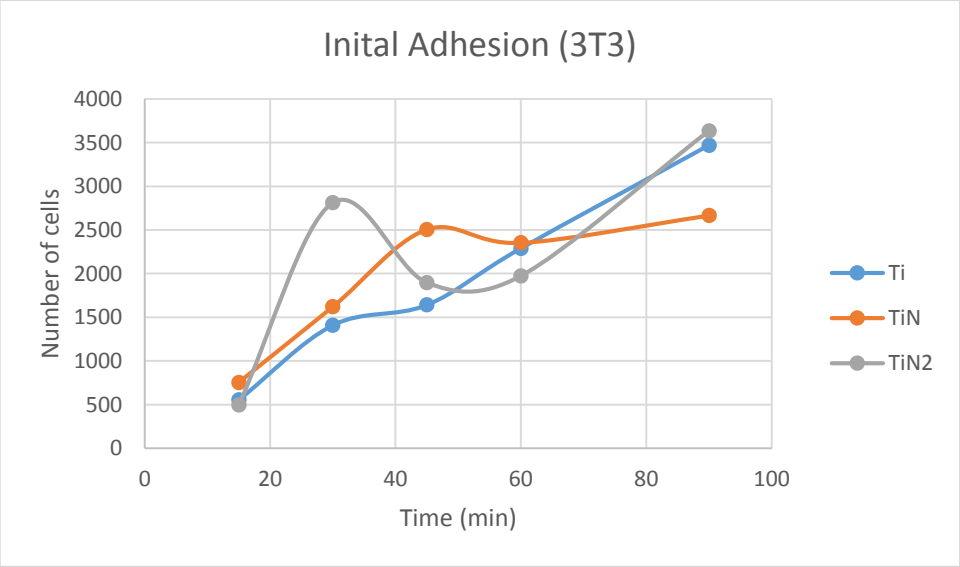

Figure 25. Adhesion of 3T3 cells to the different surfaces.

3.4.4. Wound Healing Assay

Values for all measurements collected during the wound healing experiments can be seen in appendix C.

HGF-1 Cells

Images from wound healing experiments on uncoated Ti-samples and samples coated with TiN can be seen in Figure 26. Based on this visual evaluation it can be seen that wound healing due to migration of cells seem to be faster on TiN samples. After the eight hours of the experiments the artificial wound is more healed on TiN-samples as compared to uncoated Ti-samples.

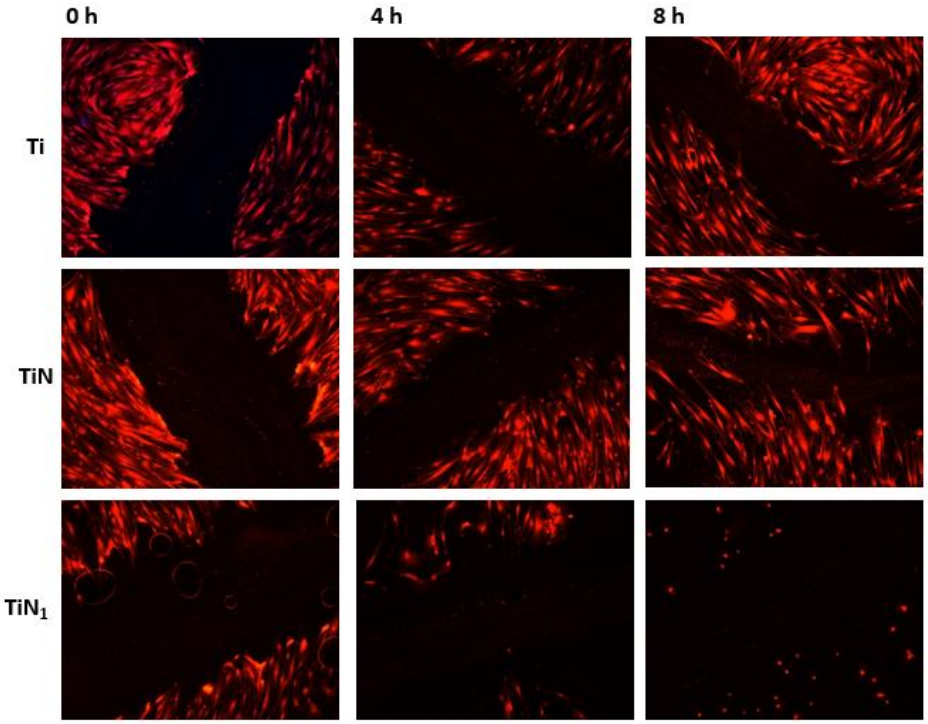

Figure 26. Images from wound healing experiments performed with HGF-1 cells on Ti, TiN and TiN_1-samples. Using a fluorescent microscope at ten times magnification.

Images in Figure 26 were evaluated using equation [1], and all calculated values of the percentage of wound healing are presented in Table 3.

Table 3. Values of x (the percentage of wound healing) calculated by equation 1.

Time	Sample:	X Ti (%)	X TiN (%)
0 h	*Average*	0	0
	St. Dev	0	0
2 h	*Average*	17	22
	St. Dev	3,6	5,8
4 h	*Average*	27	32
	St. Dev	3,1	7,9
6 h	*Average*	31	49
	St. Dev	8,4	12,8
8 h	*Average*	38	63
	St. Dev	11,8	18

The graphical representation of these values can be seen in Figure 27. A difference in the healing process can be seen between Ti- and TiN-samples already four hours into the experiment, Figure 27. After eight hours the healing is 63 % complete for cells growing on TiN-samples and 38 % complete for cells growing on Ti-samples, Table 3.

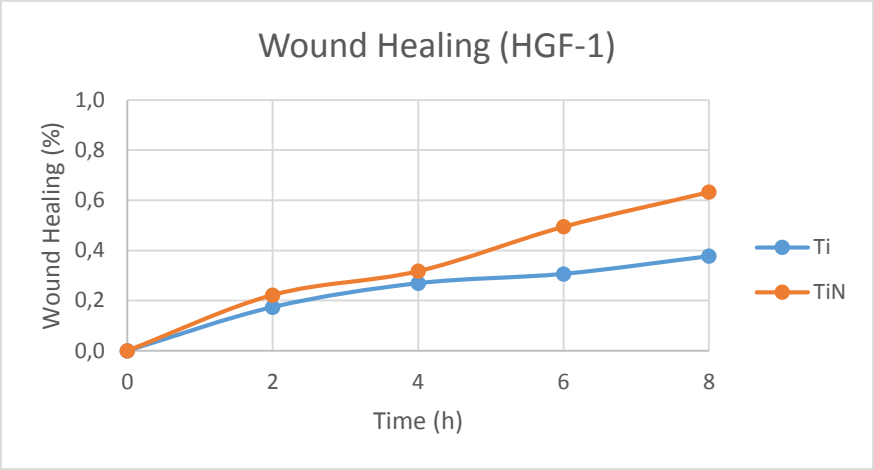

Figure 27. The graphical representation of calculated values from the wound healing experiment performed with HGF-1 cells.

Images from the wound healing experiment performed with HGF-1 on TiN_1 can also be seen in Figure 26. Due to few cells on the coins after the wound healing experiments performed with TiN_1-samples, the images could not be evaluated using equation [1].

3T3 cells

Images from wound healing experiments performed with 3T3 cells are shown in Figure 28. Wound healing experiments with 3T3 cells were performed on Ti- and TiN-samples. Attempts to perform wound healing experiments on TiN2-samples failed as confluence of 3T3 cells could not be achieved.

By studying images from the wound healing experiment, Figure 28, it can be seen that the wound healing after 8 h seems to be more complete for cells grown on samples coated with TiN as compared to uncoated Ti surfaces.

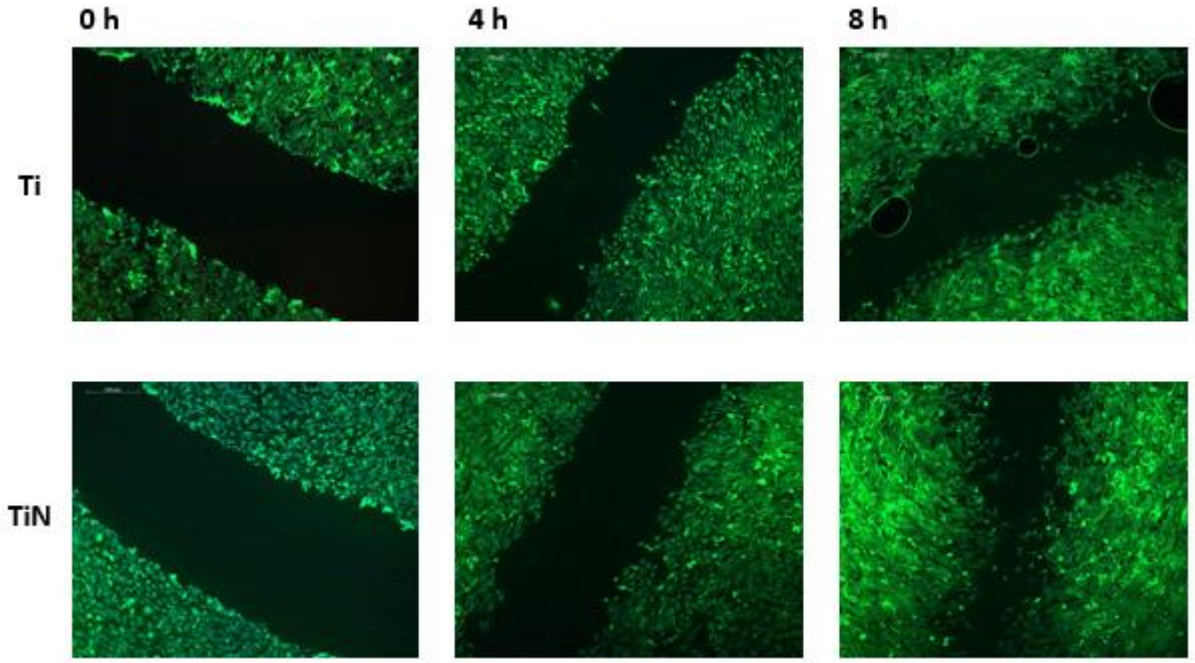

Figure 28. Images from wound healing experiments performed with 3T3 cells on Ti and TiN samples.

The calculated values (using equation [1]) are presented in Table 4

Table 4. Calculated values of X representing the percentage of wound healing.

Time	Sample:	X Ti (%)	X TiN (%)
0 h	*Average*	0	0
	St. Dev	0	0
2 h	*Average*	14	16
	St. Dev	5,4	2,1
4 h	*Average*	33	36
	St. Dev	17	6,4
6 h	*Average*	46	50
	St. Dev	12	3,7
8 h	*Average*	60	84
	St. Dev	7,8	10

When studying the graphical representation of the calculated value X, Figure 28, it can be seen that the migration of cells on samples coated with TiN and on uncoated Ti- samples is similar during the initial six hours. However, after eight hours the healing is significantly more complete on samples coated with TiN as compared to Ti-samples.

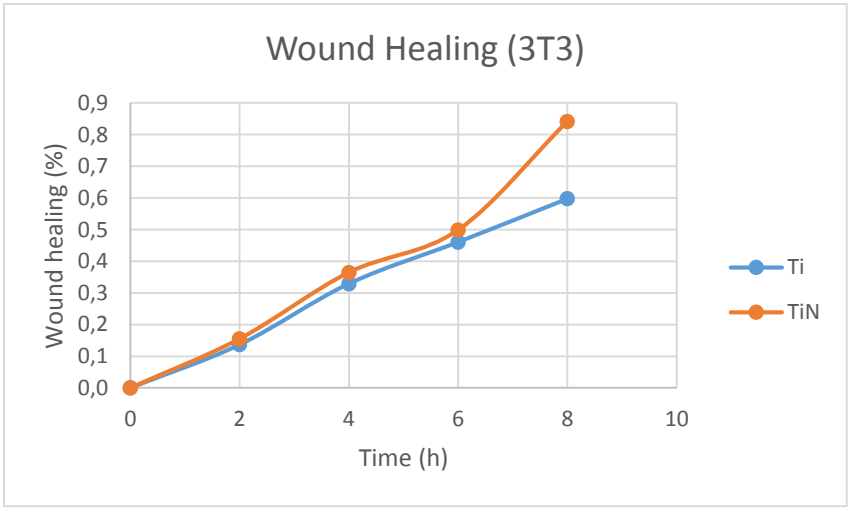

Figure 29. Graphical representation of the wound healing in percentage from wound healing experiments performed with 3T3 cells.

4. Discussion

In this study it was seen that the four different sample groups evaluated showed different surface characteristics due to chemically modified coatings. These chemical modifications also showed different *in vitro* cellular responses in terms of cell growth and migration. However, no difference between the chemically modified surfaces could be seen in the initial adhesion tests or during the SEM analysis of cell morphology.

The SEM images of the four different surfaces evaluated in this study, show that all samples have visible machining tracks seen as round circles on the samples, Figure 19. From SEM images in Figure 19 it can also be seen that the morphology of the surface of TiN_2 samples have become heterogeneous due to the chemical modifications. This can to some extent be seen for TiN_1 samples, but not for TiN samples which have homogeneous appearance, similar to uncoated Ti-surfaces. However, the profilometry measurements seen in Table 2 indicate the surface roughness to be similar for all samples (R_a=0,14 µm), except for TiN_1-samples (R_a = 0,24 µm). When evaluating these results it is necessary to consider the parameter R_a used to describe the surface roughness in this study. R_a does not provide a conclusive characterization of the surface structure as R_a only measures vertical alternations. For a complete topographical characterization parameters reflecting spatial and hybrid variations are also needed (30). Furthermore, in order to detect possible nanoscale alternations of the surfaces another analytical technique is needed, such as for example Atomic Force Microscopy (AFM).

The difference of the R_a-value for TiN_1-samples can be due the R_a-value largely being dependent on the machining tracks during the SEM-analysis, Figure 19. As TiN_1 was included later in the study the coins come from different batches which can explain the higher R_a-value. The higher R_a-value is thus not necessarily due to the chemical modification of the surface. Previous studies show that fibroblasts prefer smooth surfaces as compared to rough surfaces (4).

From contact angle measurements it can be seen that there is almost no difference in the hydrophilicity between the uncoated Ti-samples and the samples coated with TiN. However, the chemically modified TiN-samples, TiN_1 and TiN_2 show a lower wettability as compared to the Ti- and TiN-samples, see Table 1. Both TiN_1- and TiN_2-samples have a contact angle higher than 90 ˚ and can therefore be classified as hydrophobic. In terms of wanted abutments surface characteristics, hydrophobic surfaces can be disadvantageous as it can affect the protein adsorption and cell adhesion (36) (4).

The SEM-analysis of the cell morphology seen in Figure 21 show that the 3T3 cells are smaller and have a more round morphology as compared to the long cell morphology of the HGF-1 cells on Ti-samples, Figure 20. That few or no cells were seen for SEM analysis of HGF-1 cells may be due to the preparation procedure and the amount of cells used for seeding of the SEM-samples. As seen for 3T3-cells the layer of cells are thick and the machining tracks of the coins cannot be seen, Figure 21. The thick cell layer of cells prevents evaluation of the cells-coating interaction on the chemically modified coatings. For proper evaluation of cell-coating interaction fewer cells should be used for SEM-analysis.

Results from the growth study, Figure 22, shows that the growth of HGF-1 cells on chemically modified surfaces of TiN- and TiN_1-samples are comparable to cell growth on uncoated Ti-samples. It can also be seen that cells tend to grown in a circular pattern, aligning along the machining tracks of the samples (4), Figure 19. The results from the growth study are graphically presented in Figure 23 and are consistent with the visual evaluation of images in Figure 22. It can be seen that growth of

HGF-1 cells is similar for Ti, TiN and TiN1-samples. However, both Figure 22 and Figure 23 show that chemically modified TiN_2-samples cannot support cell growth.

Results from the initial adhesion tests showed no significant difference in cell adhesion 90 minutes after seeding, for either HGF-1 cells, Figure 24, or 3T3-cells, Figure 25. As discussed previously in the report the initial adhesion of cells to an abutment surface is significant in order to reduce the risk of infections (6). Based on the results from the initial adhesion study, it can be assumed that the number of cells adhering to the different samples during the growth study is similar. The results from the growth study seen for TiN_2, see Figure 22, can therefore be assumed to be mainly related to poor cell growth and not to differences in the initial adhesion.

During the wound healing experiments the same observations were seen for both 3T3 cells and HGF-1 cells, that the wound healing process were more complete on surfaces coated with TiN compared to uncoated Ti surfaces, see Figure 26 and Figure 28. When evaluating the results from the wound healing experiments performed with HGF-1 cells using equation [1], a graphical representation of the wound healing process was obtained, see Figure 27. This graph show the percentage of wound healed, where a 100 % represents a fully healed wound. As can be seen in Figure 27 a difference between HGF-1 cells on Ti- and TiN-samples can be seen six hours into the experiment. Eight hours into the experiment the wound healing of HGF-1 are 60 % complete on TiN-surfaces and 38% complete on Ti-surfaces, see Table 3. This indicates that cells are more prone to migration on TiN-surfaces as compared to uncoated Ti-surfaces. When observing the images of the wound healing after eight hours another observation can be made, Figure 26, on TiN-samples cells from different sides of the gap have started to make contact (d_t=0), this was never observed on the Ti-samples. These results indicate that HGF-1 cells on TiN-surfaces are capable of closing a wound faster as compared to HGF-1 cells on uncoated Ti-samples.

The same trend as observed for HGF-1 cells could be seen for 3T3-cells during the wound healing experiments, Figure 28. However, the difference in healing between the surfaces could only be seen eight hours into the experiment, see Figure 29. Eight hours into the experiment the wound healing were 84 % complete on TiN-samples as compared to Ti-samples, 60 %, see Table 4. Overall the wound healing was less complete for experiments performed with HGF-1 cells as compared to experiments performed with 3T3 cells, see Figure 29 and Figure 27.

The trend seen for both cell types during the wound healing experiments is that cells migrate faster on TiN-samples than on Ti-samples. This indicates that coatings of TiN would provide a more suitable surface for dental abutments as compared to uncoated Ti abutments. And that cells in contact with a TiN-coatings may be capable of closing a wound faster and thus provide a shorter healing time. Another observation seen for both cell types is that the healing process seems to speed up when the different sides of the wound starts to get in contact. For 3T3 cells this was seen after six hours, see Figure 29, but for HGF-1 cells this trend was seen already after four hours, see Figure 27. This observation could be due to the long cell shape of the HGF-1 cells, see Figure 20, 3T3 cells have a more round cell shape, see Figure 21. The long cell shape of the HGF-1 cells could potentially enable the cells to easier communicate across the wound.

Wound healing experiments could not be successfully performed on samples coated with chemically modified titanium nitride coatings, TiN_1 and TiN_2-samples, results from TiN_1-samples are presented in Figure 26. Wound healing experiments on TiN_2-samples could not be performed as the surface were unable to support cell growth to a confluent layer of cells which is necessary for wound healing experiments, see Figure 23. According to results from the growth study TiN_1-samples are capable of supporting cell growth, but when evaluating wound healing experiments for TiN_1-samples few cells

were found on the coins. Pennisi et al (37) shows that a minor reduction of the migration potential for fibroblasts can be related to a higher surface roughness. However, the lack of cells could be due to cells having a higher adhesion between the cells than to the metallic coins. If so, the entire cell population on the coin would be removed during scratching at the start of the experiment. This could explain why no cells could be found during the wound healing experiment with TiN_1-samples, see Figure 26. For a proper explanation evaluation of cell adhesion and cell adhesion points should be performed and compared to the other surfaces. This could be done by using immunohistochemistry and staining of vinculin and thus marking focal adhesions between the cells and the coin.

The wound healing seen during the experiments are mainly due to cell migration, as cell division would have been a minor contribution during experiment considering the time frame of the experiment. The method of evaluating the results from the wound healing experiments by measuring d_t and d_0 provides a good measure of the cells' capability of migrating to close a wound. However, the calculated values become less accurate with time as d_0 becomes harder to determine. However, the calculated values, see Table 4 and Table 3, are consistent with the visual evaluation of the images in Figure 28 and Figure 26 and thus these calculations can be considered to be a relevant evaluation of the results. As the same trends have been seen for multiple repeats of the wound healing experiments, it can be concluded that the wound healing is more complete for TiN-coated samples compared to uncoated Ti-samples. However, the extent of the healing varies from samples to sample. Especially for TiN-samples as some points along the wound have contact across the gap (d_t=0), whereas other parts of the wound have larger d_t values.

Wound healing experiments is a common method of evaluating cell migration and the cells ability to close an artificial wound (35). However, wound healing experiments on metallic surfaces are rare. The *in vitro* evaluation of the wound healing potential can serve as a useful indication of the interaction between the surface coating and the cells.

In this study fibroblasts were used for evaluation of different abutments surfaces *in vitro*. In the *in vivo* situation fibroblast are not in direct contact with the abutment surface, but they are a part of the connective tissue surrounding the abutment. And the fibroblasts are responsible for producing the extracellular matrix in the connective tissue and plays an important role during the healing process (4). The fibroblasts role of preventing bacterial adhesion has also been considered important (24). The cell and bacterial adhesion is believed to be largely related to the surface characteristic of the surface. For the four surface groups evaluated in this study, it can be seen that the chemical modification of the titanium surface changes the surface characteristic in terms of morphology, wettability and chemical composition. The four surface groups also show different cellular responses in terms of growth, adhesion and migration. However, it is difficult to say what surface characteristic is mainly responsible for the difference in cellular response.

Based on the results in this study it can see that the change of surface characteristic can change the cellular response *in vitro*. Results based on an *in vitro* model can serve as a useful tool when evaluating a large number of potential surface coating candidates. The *in vitro* model is a first step in evaluating the suitability of the surface coating for application in dental abutments. However, in order to fully evaluate the surface coatings further studies are necessary, such as *in vivo* and clinical studies. The results in this study indicated that TiN-coatings are able to support cell growth, adhesion and migration which indicate that it is a suitable surface coating for dental abutment.

5. Conclusion

In this study chemically modified titanium surfaces were evaluated in terms of surface characteristics and the cellular response *in vitro*. The *in vitro* study aimed to determine the cell growth, migration and initial adhesion to the chemically modified coatings. Based on the results in this work the following conclusions can be made:

- Surface characterization of the different coatings showed that the chemical modifications altered the surface characteristics of the samples. The wettability was reduced for all chemically modified titanium nitride surfaces as compared to uncoated titanium surfaces and TiN-surfaces. A change in the surface morphology due to the chemical modifications can be seen for TiN_2-samples. The surface roughness (R_a-values) was similar for all samples, except for TiN_1-samples which showed a higher surface roughness.

- The chemical modifications of the surfaces also showed different cellular responses *in vitro*, in terms of cell growth and migration. No difference between 3T3-cells or HGF-1-cells could be seen in initial adhesion tests, nor in the morphology of the 3T3-cells based on the SEM-analysis. The growth study performed using HGF-1-cells showed no difference in cellular growth when comparing TiN- and TiN_1-samples to uncoated Ti-samples. However, cell growth was not supported by the TiN_2-samples. Cell migration was faster on TiN-samples as compared to Ti-samples, based on results from wound healing experiments performed with both cell types respectively. Wound healing experiments could not be performed with either TiN_1-samples or TiN_2, possibly due to poor adhesion.

- Based on the results in this study TiN-coatings seem to be best suitable for application in dental abutments. This is based on results from cell growth and migration studies *in vitro* which indicates potential for fibroblasts in the connective tissue to close a wound surrounding a TiN coated dental abutment *in vivo*.

6. References

1. **Pye A D, Lockhart D E A, Dawson M P, Murray C A, Smith A J.** A review of dental implants and infection. *Journal of Hospital Infection.* June 2009, pp. 104-110.

2. **Johnson T, Wood D J.** *Techniques in Complete Denture Technology.* s.l. : Johan Wiley & Sons, 2012. ISBN 9781405179096.

3. *Osseointegration in skeletal reconstruction and rehabilitation: A review.* **Branemark R, Branemark P I, Rydevik B, Myers R R.** 2001, Journal of Reabilitation Research and Development, pp. 175-181.

4. *The effects of material characteristics, of surface topography and of implant components and connections on soft tissue intefration: a litterature review.* **Rompen E, Domken O, Degidi M, Farias Pontes A E, Piattelli A.** 2006, Clinical Oral Implant Research, pp. 55-67.

5. *Saucerization of osseointegrated implants and planning of stimultaneous orthodontic cinical cases.* **Consolaro A, de Carvalho R S, Francischone Jr C E, Consolaro M F M O, Francischone C E.** 2010, Dental Press J Orthod, pp. 19-30.

6. *In vivo study of the initial bacterial adhesion on different implant materials.* **Al-Ahamd A, Wiedmann-Al-Ahmad M, Fackler A, Follo M, Helwig E, Bächle M, Hannig C, Han J-S, Wolkewitz M, Kohal R.** 2013, Archive of Oral Biology, pp. 1139-1147.

7. *Inital attachment, subsequent cell proliferaion/viability and gene expression of epithelial cellls realted to attachment and wound healing in response to different titanium surfaces.* **An N, Rausch-Fan X, Wieland M, Matejka M, Andrukhov O, Schedle A.** 2012, Dental Materials, pp. 1207-1214.

8. *Human Gingical Fibroblasts (HGF-1) Attachments and Proliferation on Several Abutment Materials with Various Colors.* **Kim Y-S, Ko Y, Kye S-B, Yang S-M.** 2014, The International JOurnal of Oral & Maxillofacial Implants, pp. 969-975.

9. *Soft tissue integration versus early biofilm formation on different dental implant materials.* **Zhao B, Van der Mei H C, Subbiahdoss G, de Vries J, Rustema-Abbing M, Kuijer R, Busscher H J, Ren Y.** 2014, Dental Materials, pp. 716-727.

10. *Is keratinized mucosa indespensible to maintain peri-implant health? A systematic review of the literature.* **Brito C, Tenenbaum H C, Wong B K C, Schmitt C, Nogueira-Fihlo G.** 2014, Journal of biomedical materials researchB: Applied Biomaterials , pp. 643 - 650.

11. *Biofilms.* **López D, Vlamakis H, Roberto K.** Boston : Cold Spring HArb Perspect Biol 2012;2:a000398, 2010. doi: 10.1101/cshperpect.a000398.

12. **Belcarz A, Bieniás J, Surowska B, Ginalska G.** Studies of bacterial adhesion on TiN, SiO2-TiOs and hydroxyapatite thin layers deposited on titanium and Ti6Al4V alloy for medical applications. *Thin Solid films.* 2010, pp. 797-803.

13. *Plaque formation on surface modified dental implants. An in vitro study.* **Grossner-Schreiber B, Gripentrog M, Haustein I, Muller WD, Lange KP, Breidigkeit H, Göbel UB.** s.l. : Clin. Oral Impl. Res., 2001, Vols. (12) 543-551. ISSN: 0905-7161.

14. **Tortora G J, Reynolds Grabowski S.** *Priniciples of anatomy and physiology, eighth edition.* New York : HarperCollins Collage Publishers, 1996.

15. *A Comparison of Epithelial Cells, Fibroblasts, and Osteoblasts in Dental Implant Titanium Topographies .* **Teng F-Y, Ko C-L, Kuo H-N, Hu J-J, Lin J-H Lou C-W, Hung C-C Wang Y-L, Cheng C-Y Chen W-C.** 2012, Bioinorganic Chemistry and Applications , p. Article ID 687291.

16. *The mucosal attachment to titanium implants with different surface characteristics: an experimental study in dogs.* **Abrahamsson I, Zitzmann N U, Berglundh T, Linder E, Wennerberg A, Lindhe J : Blackwell Munksgaard, 2002, Vols. 29: 448-455.**

17. *Epithelial Attachment and Downgrowth on Dental Implant Abutments - A Comprehensive Review.* **Iglhaut G, Schwarz F, Winter R R, Mihatovic I, Stimmelmayr M, Schliephake H. 2014, Journal of Esthtic and Restorative Dentistry, pp. 324-331.**

18. *ERM functions, EGF and orthodontic movement.* **Consolaro A, Consolaro M F M-O. 2010, Dental Press J. Orthod., pp. 24-32.**

19. *Modulation of cell adhesion, proliferation and differentiation on materials designed for body implants.* **Bacakova L, Filova E, Parizek M, Ruml T, Svorcik. 2011, Biotechnology Advances , pp. 739-767.**

20. Alberts B, Johanson A, Lewis J, Raff M, Roberts K, Walter P. *Molecular Bilogy of the cell - Fifth edition.* **New York : Garland Science, Taylor & Francis Group, LCC, 2008. ISBN: 978-0-8153-4106.**

21. Altankov G, Grinnell F, Groth T. Studies on the biocompatibility of materials: Fibroblast reorganization of substratum-bond fibronectin on surfaces varying on wettability. ***Journal of Biomedical Materials Research.*** **1996, Vol. 30, p.385-391.**

22. *Effect of surface processing on the attachment, orientation, and proliferation of humna gingival fibroblasts on titanium.* **Kononen M, Hormia M, Kivilahti J, Hautaneimi J, Thesleff I. 1992, Journal of Biomedical Materials Research, pp. 1325-1241.**

23. *Immunolocalization of proteins specific for adhaerens junctions in human gingival epithelial cells grown on differently processed titanium surfaces.* **Hormia M, Kononen M, Kivilathi J, Virtanen I. 1991, Journal of Periodontal Research, pp. 491-497.**

24. *In vitro Biocompatibility of New Silver (I) Coordination Compound Coated-Surfaces for Dental Implant Applications.* **Brunetto P S, Slenters T V, Katharina M F. 2011, Materials, pp. 355-367.**

25. *Bacterial Adhesion on Titanium Nitride-Coated and Uncoated Implants: An in vivo Human Study.* **Scarano A, Piattelli M, Vrespa G, Caputi S, Piattelli A. 2003, Journal of Oral Implantology, pp. 80-85.**

26. Mattox, Donald M. *Handbook of Physical Vapor Desposition (PVD) Processing (2nd Edition).* **s.l. : Elsevier, 2012. Electronic ISBN: 978-0-8155-2038-2.**

27. *Ionized physical vapor deposition of titanium nitride: A global plasma model.* **Tao K, Mao D, Hopwood J. 7, Boston : Journal of Applied Physics, 2002, Vol. 91. doi: 10.1063/1.1455139.**

28. Wild P G, Qin W. *Nanotechnology Research Methods for Foods and Bioproducts.* **Hoboken, NJ, USA : John Wiley & Sons. , 2012.**

29. *Contact angel measurement and contact angle interpretation.* **Kwok D Y, Neumann A W. Toronto : Advances in Colloid and Interface Science, 1999, Vols. 167-249.**

30. T, Thomas R. *Rough Surfaces.* **London : Imperial Collage Press, 1999. ISBN 1-86094-1.**

31. *Characterization of surface roughness.* **Thomas T, R. 1981.**

32. Gray W, Jerome J, Price R L. *Basic Confocal Microscopy.* **s.l. : Springer New York , 2011. Online ISBN: 978-0-387-78175-4.**

33. Berg J M, Tymoczko J L, Stryer L. *Biochemistry.* **New York, US : W. H. Freeman and Company, 2007.**

34. Sigma-Aldrich. Sigma-Aldrich. *DAPI for nucleic acid staining.* **[Online] 2015. [Cited: Feb 02, 2015.] http://www.sigmaaldrich.com/catalog/product/sigma/d9542?lang=en&region=SE.**

35. *Differential response of human ginigval fibroblasts to titanium- and titanium-zirconium-modified surfaces* **. Gómes-Florit M, Ramis JM, Xing R, Taxt-Lamolle S, Haugen HJ, LYngstadaas S P, Monjo M. 2013, JOurnal of periodontal research, pp. 425-436.**

36. *Relationship between surface properties (roughness, wettability) of titanium and titanium alloys and cell behaviour.* **Ponsonnet L, Reybier K, Jaffrezic N, Comte V, Lagneau C, Lissac M, Martelet C. s.l. : Materials Science and Engineering , 2003, Vols. 551-560.**

37. *Nanoscale topography reduces fibroblast growth, focal adhesion size and migration-related gene expression on platinum surfaces.* **Pennisi C P, Dolatshashi-Pirouz A, Foss M, Chevallier J, Fink T, Zachar V, Besenbacher F, Yoshida K. s.l. : Colloids and Surfaces B: Biointerfaces, 2011, Vols. (85) 189-197. doi: 10.1016/j.colsurfb.2011.02.28.**

Appendices

Data from initial adhesion tests and wound healing experiments are presented in the following sections.

A. Results from growth study

During the growth study both DAPI and phalloidin were used for staining and thus also used for color marking in *Photoshop*. Results and the obtained values are presented in Table 5.

Table 5. Results from growth study performed with HGF-1 cells on all sample groups, two coins for each day and sample group were evaluated.

Sample group		Day 1	Day 2	Day 3	Day 4	Day 5
Ti	DAPI	382	614	828	1075	1668
	Phalloidin	485	712	1281	1355	1724
	DAPI	-	-	-	-	-
	Phalloidin	996	1783	1579	1381	1612
	Average	***612***	***1036***	***1229***	***1270***	***168***
TiN	DAPI	529	644	964	988	1152
	Phalloidin	610	714	1218	1219	1379
	DAPI	-	-	-	-	-
	Phalloidin	1167	2046	1565	1393	1355
	Average	***769***	***1135***	***1249***	***1200***	***1295***
TiN_1	DAPI	313	658	801	1098	1150
	Phalloidin	469	682	917	1294	1481
	DAPI	-	-	-	-	-
	Phalloidin	626	1748	1326	1072	1432
	Average	***469***	***1029***	***1015***	***1154***	***1354***
TiN_2	DAPI	-	457	207	205	
	Phalloidin	312	479	357	337	236
	DAPI	-	-	-	-	-
	Phalloidin	33	197	32	63	49
	Average	***173***	***378***	***199***	***202***	***143***

B. Results from initial adhesion study

Results from studies with HGF-1 and 3T3-cells are presented below.

HGF-1 cells

Results from the initial adhesion tests performed with HGF-1 cells. Results from three separate experiments are presented below, see Table 6.

Table 6. Results from the initial cell adhesion tests with HGF-1 cells.

Time (min)	Ti	TiN	TiN_2
15,00	6	12	4
	10	15	10
	4	8	5
	20	**35**	**19**
30,00	93	97	137
	25	72	63
	122	172	216
	240	**341**	**416**
45,00	213	148	244
	206	217	313
	367	294	432
	786	**659**	**989**
60,00	79	319	351
	295	754	311
	411	338	429
	785	**1411**	**1091**
90,00	509	231	334
	605	828	408
	461	509	679
	1665	**1568**	**1421**

3T3 cells

Results from the initial adhesion studies performed with 3T3-cells. Results from three separate measurements are shown below, Table 7

Table 7. Results from initial adhesion tests with 3T3 cells.

Time (min)	Ti	TiN	TiN_2
15,00	789	387	645
	534	480	565
	338	1389	270
	534	**752**	**496**
30,00	1345	609	1369
	338	1792	5212
	2542	2455	1824
	1408	**1619**	**2811**
45,00	234	1450	1058
	1313	1823	3425
	3376	4241	1208
	1641	**2505**	**1897**
60,00	1543	2111	796
	2376	1690	2889
	2946	3256	1208
	2288	**2352**	**1973**
90,00	1265	1053	1083
	3329	1448	4008
	5811	5492	5812
	3468	**2664**	**3634**

C. Results from wound healing assay

Results from the wound healing assays performed with HGF-1 and 3T3-cells are presented below.

HGF-1 cells

All measuring points from the wound heling assays with HGF-1 cells are presented in the Table 8. Results from three different experiments are shown, as well as the calculated value X.

Table 8. Results from wound healing experiments with HGF-1 cells.

	Time (h)	Ti d_0 (µm)	Ti d_t (µm)	TiN d_0 (µm)	TiN d_t (µm)
Experiment 1	**0**	573,15	573,15	716,30	716,30
		643,45	643,45	567,11	567,11
		655,03	655,03	707,16	707,16
		581,54	581,54	605,10	605,10
		543,79	543,79	614,74	614,74
		588,20	588,20	595,02	595,02
	Average:	*597,53*	*597,53*	*634,24*	*634,24*
Experiment 2	**0**	624,11	624,11	609,48	609,48
		674,17	674,17	574,84	574,84
		662,01	662,01	640,09	640,09
		762,17	762,17	576,47	576,47
		662,44	662,44	630,71	630,71
		740,05	740,05	600,37	600,37
	Average:	*687,49*	*687,49*	*605,33*	*605,33*
Experiment 3	**0**	515,14	515,14	607,94	607,94
		628,50	628,50	620,64	620,64
		610,17	610,17	622,80	622,80
		506,90	506,90	479,75	479,75
		470,09	470,09	587,94	587,94
		645,59	645,59	647,36	647,36
	Average:	*562,73*	*562,73*	*594,41*	*594,41*
	X=1-d_t/d_0		***0,00***		***0,00***
Experiment 1	**2**	696,99	572,79	558,38	464,63
		695,42	571,48	603,80	493,58
		663,62	559,25	589,36	463,49
		524,17	450,37	692,36	545,95
		558,22	492,69	611,72	442,88
		549,51	547,94	629,51	440,17
	Average:	*614,66*	*517,42*	*614,19*	*475,11*
Experiment 2	**2**	717,09	570,47	662,15	485,03
		702,98	603,50	671,69	535,22
		677,67	584,77	573,11	452,60
		723,29	585,50	510,99	445,20
		737,77	633,88	472,02	428,90
		795,55	569,40		
	Average:	*725,73*	*606,25*	*577,99*	*469,39*
Experiment 3	**2**	653,39	508,39	777,23	614,52
		666,16	524,56	831,39	607,32
		633,01	469,50	853,04	580,12
		566,81	451,42	667,02	498,74
		659,13	576,89	647,80	481,52
		610,13	496,28	596,94	466,03
	Average:	*631,52*	*504,51*	*728,90*	*541,37*
	X=1-d_t/d_0		**0,1740**		**0,2224**

	Time (h)	Ti d_0 (µm)	Ti d_t (µm)	TiN d_0 (µm)	TiN d_t (µm)
Experiment 1	**4**	541,10	403,89	690,44	438,48
		564,11	445,24	754,80	406,30
		566,23	391,37	709,25	395,44
		625,00	446,56	750,20	471,16
		600,25	424,59	850,59	537,02
		549,19	394,17	748,54	434,27
	Average:	*574,31*	*417,64*	*750,64*	*447,11*
Experiment 2	**4**	1159,07	868,33	1234,15	901,25
				1161,79	839,52
				1119,65	795,02
				1247,06	1084,99
				999,08	745,96
				960,51	642,28
	Average:	*1159,07*	*868,33*	*1120,37*	*834,84*
Experiment 3	**4**			586,60	418,18
				589,44	399,15
				595,65	418,63
				510,44	388,82
				568,16	372,36
				455,21	346,49
	Average:			*550,92*	*390,60*
	X=1-d_t/d_0		***0,2692***		***0,3172***
Experiment 1	**6**	751,96	433,42	775,69	439,74
		659,17	348,53	786,93	377,20
		641,32	379,93	753,87	401,61
		668,69	431,50	699,37	342,17
		630,76	404,54	831,54	377,54
		577,52	394,93	781,32	366,17
Average:	*Average:*	*654,91*	*398,81*	*771,45*	*384,07*
Experiment 2	**6**	1275,16	1054,10	1162,85	758,46
		1229,41	1018,03	1119,33	698,91
		1236,23	992,21	1156,67	740,98
		817,13	608,85		
		792,80	584,98		
Average:	*Average:*	*1070,14*	*851,64*	*1146,28*	*732,79*
Experiment 3	**6**	525,08	360,80	561,67	109,01
		433,47	274,94	382,77	180,21
		573,43	408,12	447,96	129,06
		488,80	330,54	529,48	235,33
		601,59	412,67	530,01	334,30
		523,46	409,38	533,85	344,20
	Average:	*524,30*	*366,08*	*497,62*	*222,02*
	X=1-d_t/d_0		***0,3067***		***0,4946***
Experiment 1	**8**	742,11	342,92	678,52	108,31
		721,80	397,34	703,87	67,84
		755,75	347,01	675,65	151,18
		820,74	415,53	803,00	55,97
		802,02	419,28	708,00	147,64
		708,76	388,89	801,99	120,86
	Average:	*758,53*	*385,16*	*728,61*	*108,63*

	Time (h)	Ti d_0 (µm)	Ti d_t (µm)	TiN d_0 (µm)	TiN d_t (µm)
Experiment 2	**8**	1116,82	659,66	1199,44	555,20
		1077,26	814,47	1198,19	484,57
		1194,24	907,71	1079,63	508,85
		1222,19	1031,38	945,53	634,44
		1202,08	961,49	1096,59	677,39
		1248,76	998,11	957,25	581,72
	Average:	*1176,89*	*895,47*	*1079,44*	*573,70*
Experiment 3	**8**	589,04	348,05	729,12	337,50
		558,57	304,50	700,56	229,95
		468,23	255,47	573,80	271,66
		462,77	305,64	498,74	161,64
		443,32	271,12	471,63	229,94
		442,19	291,36	427,30	165,55
	Average:	*494,02*	*296,02*	*566,86*	*232,71*
	X=1-d_t/d_0		***0,3771***		***0,6329***

3T3 cells

Results from all measuring points from the wound healing assay performed with 3T3 cells is presented in Table 9 below.

Table 9. Results from wound healing experiments performed with 3T3 cells.

	Time (h)	Ti d_0 (µm)	Ti d_t (µm)	TiN d_0 (µm)	TiN d_t (µm)
Experiment 1	**0**	547,06	547,06	-	-
		508,67	508,67	-	-
		538,97	538,97	-	-
		597,84	597,84	-	-
		563,92	563,92	-	-
		521,52	521,52	-	-
	Average:	*546,33*	*546,33*		
Experiment 2	**0**	-	-	-	-
		-	-	-	-
		-	-	-	-
		-	-	-	-
		-	-	-	-
		-	-	-	-
	Average:				
	X=1-d_t/d_0		***0,00***		***0,00***
Experiment 1	**2**	529,13	388,33	537,77	440,86
		521,59	457,99	522,56	457,08
		425,87	364,67	541,65	458,59
				537,89	431,99
				535,09	451,18
				526,60	454,05
	Average:	*492,20*	*403,67*	*533,59*	*449,05*
Experiment 2	**2**	548,62	469,23	593,15	498,07
		525,22	469,75	600,88	513,67
		494,39	447,59	531,45	453,63
		521,32	430,68	615,55	537,87
		490,67	449,44	635,39	536,66
		520,28	470,95	600,27	492,87
	Average:	*516,75*	*456,27*	*596,12*	*505,46*
	X=1-d_t/d_0		***0,1366***		***0,1551***

	Time (h)	Ti d_0 (µm)	Ti d_t (µm)	TiN d_0 (µm)	TiN d_t (µm)
Experiment 1	**4**	371,88	166,94	533,40	317,93
		346,59	131,64	493,48	324,05
		316,28	129,06	496,82	338,10
		285,64	163,66	506,98	319,83
		308,28	222,77	480,32	287,89
		387,50	250,64	455,47	235,32
	Average:	*336,03*	*177,45*	*494,47*	*303,85*

	Time (h)	Ti d_0 (µm)	Ti d_t (µm)	TiN d_0 (µm)	TiN d_t (µm)
Experiment 2	**4**	504,73	429,11	633,96	482,73
		406,92	*341,07*	665,64	437,05
		432,32	353,76	583,11	414,32
		454,14	367,01	511,07	280,74
		451,30	337,27	605,15	379,71
		451,70	365,77	639,02	407,68
	Average:	450,18	365,67	*606,33*	*400,37*
	X=1-d_t/d_0		***0,3291***		***0,3647***
Experiment 1	**6**	530,36	175,56	574,80	253,20
		630,45	235,62	646,74	334,73
		525,74	249,42	652,13	325,22
		517,44	265,45	675,59	336,23
		546,11	226,52	612,89	306,41
		512,17	250,59	546,54	281,99
Average:	*Average:*	*543,71*	*233,84*	*618,11*	*306,30*
Experiment 2	**6**	568,26	298,93	636,41	287,90
		570,28	352,03	703,27	351,08
		584,45	407,93	724,34	427,66
		498,20	334,99	739,57	387,08
		519,61	368,96	796,82	371,66
		504,08	328,24	818,61	416,52
Average:	*Average:*	*540,81*	*348,51*	*736,50*	*373,65*
	X=1-d_t/d_0		***0,4608***		
Experiment 1	**8**	582,09	287,53	706,42	269,38
		619,82	310,40	655,85	83,11
		590,82	220,90	593,74	60,30
		512,15	141,04	676,40	44,57
		591,91	212,27	709,85	121,41
		611,93	251,64	730,50	73,10
	Average:	*584,79*	*237,30*	*678,79*	*108,65*
	X=1-d_t/d_0		***0,1314***		***0,8422***